Disordered Alloys and Their Surfaces: The Coherent Potential Approximation

I. Turek[1], J. Kudrnovský[2], and V. Drchal[2]

[1] Institute of Physics of Materials, Academy of Sciences of the Czech Republic, Žižkova 22, CZ-616 62 Brno, Czech Republic
[2] Institute of Physics, Academy of Sciences of the Czech Republic, Na Slovance 2, CZ-182 21 Praha 8, Czech Republic

Abstract. A recently developed ab initio approach to the electronic structure of substitutionally disordered alloys and their surfaces is reviewed. It is based on (i) the tight-binding linear muffin-tin orbital (TB-LMTO) method in the atomic sphere approximation which provides a physically transparent solution of the one-electron problem in metallic materials, (ii) the coherent potential approximation (CPA) for a mean-field treatment of the substitutional randomness, and (iii) the surface Green functions for a proper description of the true semi-infinite geometry of surfaces and interfaces. Theoretical formulation of fundamental electronic quantities, both site-diagonal (charge densities, densities of states) and site non-diagonal (the Bloch spectral functions) is presented. Transformation properties of the LMTO-CPA theory as well as specific problems of application of the local density approximation to random alloys are briefly discussed and basic algorithms employed in the numerical implementation of the formalism are described.

1 Introduction

Recent ab initio investigations of electronic properties of solids rely on the local spin-density approximation (LSDA) to the density-functional formalism and on a number of techniques solving the corresponding one-electron Schrödinger (Kohn-Sham) eigenvalue problem. These techniques comprise, e.g., the Korringa-Kohn-Rostoker (KKR) method [1,2], the linear muffin-tin orbital (LMTO) method [3,4], the linear augmented plane-wave (LAPW) method [3,5], or the optimized linear combination of atomic orbitals (LCAO) method [6]. They provide a reasonable description of the electronic structure for most of metallic solids even within the muffin-tin model [1,2] or the atomic sphere approximation (ASA) [3,4]. Full-potential versions of these techniques yield in principle an exact solution to the Schrödinger equation which is indispensable for accurate evaluation of total energies, forces, and other important quantities for perfect bulk solids (elemental metals, ordered alloys) as well as their defects (impurities, surfaces, grain boundaries).

Substitutionally disordered alloys (substitutional solid solutions) represent a broad class of systems where the above mentioned methods are only partially successful: their direct application requires large supercells simulating the randomness of real alloys. The coherent potential approximation (CPA) – introduced three decades ago [7] in terms of the Green functions – offered an

H. Dreyssé (Ed.): Workshop 1998, LNP 535, pp. 349–378, 1999.

effective-medium (mean-field) approach to the electronic structure of random alloys. Further development of the CPA was formulated first in a tight-binding picture (TB-CPA) [8,9] followed by the KKR-CPA theory [10,11] (for a review of both approaches see, e.g., [2]). In the early 1980's, the KKR-CPA became a theory of random alloys fully comparable to the existing charge selfconsistent techniques for non-random systems. The development of the TB-CPA continued towards an ab initio level which was motivated by a need for a physically simple description of the electronic structure of bulk alloys and their surfaces. This effort led to the LCAO-CPA [12,13] and the LMTO-CPA [14,15] methods which can be considered as alternatives to the KKR-CPA.

In this contribution a brief theoretical background of the LMTO-CPA method is given together with numerical techniques used in practice. The theory is developed within the TB-LMTO-ASA method [16,17] which results in an efficient unified scheme for the electronic structure of random and ordered bulk alloys, their surfaces and interfaces. Its full detailed description was presented in [15] while the numerical algorithms were reviewed in [18]. The paper is organized as follows. Section 2 summarizes the most important relations of the TB-LMTO-ASA method in terms of the Green functions. Section 3 is the central part of the paper: it introduces the concept of configurational averaging and describes the theoretical and numerical aspects of the LMTO-CPA method. Section 4 presents a short review of quantities and techniques for a treatment of layered systems (surfaces and interfaces). Section 5 deals with the application of the LSDA to random alloys. Finally, a brief survey of existing results and further extensions of the method is given in Sect. 6.

It should be noted that the LMTO-CPA formalism bears strong similarities with the KKR-CPA theory within the ASA, so that expressions for many quantities (e.g., densities of states, electronic charge densities) are fully analogous in both approaches. However, there are differences as well which arise from different Hilbert spaces and Hamiltonians: the KKR theory is based on the Hamiltonian $H = -\Delta + V(\boldsymbol{r})$ acting in the Hilbert space of functions $\psi(\boldsymbol{r})$, where $\boldsymbol{r}$ is a three-dimensional continuous variable, whereas the LMTO theory uses a local basis set with a finite number of orbitals per lattice site. The Hamiltonian is then a matrix quantity. Despite the fact that the spectra of both Hamiltonians are in principle identical (in a limited energy interval), some quantities (e.g., the Bloch spectral functions) become non-equivalent in the two approaches. From the point of view of the alloy theory, both formulations have their own merits: the Hilbert space of the KKR-CPA is explicitly non-random (independent of a particular alloy configuration), the TB (matrix) formulation of the LMTO-CPA offers, e.g., a simple perturbative treatment of relativistic effects (spin-orbit coupling) or an inclusion of many-body effects in terms of the intraatomic Coulomb and exchange integrals, etc.

2 Green Functions in the Atomic Sphere Approximation

The solution of the one-electron Schrödinger equation with a potential $V(\boldsymbol{r})$ can be equivalently formulated in terms of the one-electron Green function $G(\boldsymbol{r},\boldsymbol{r}';z)$ defined (with spin variables omitted) by [1,2]

$$\begin{aligned}[\, z \;+\; \Delta_{\boldsymbol{r}} \;-\; V(\boldsymbol{r})\,]\; G(\boldsymbol{r},\boldsymbol{r}';z) \;&=\; \delta(\boldsymbol{r}-\boldsymbol{r}')\;,\\ [\, z \;+\; \Delta_{\boldsymbol{r}'} \;-\; V(\boldsymbol{r}')\,]\; G(\boldsymbol{r},\boldsymbol{r}';z) \;&=\; \delta(\boldsymbol{r}-\boldsymbol{r}')\;,\end{aligned} \tag{1}$$

where z denotes a complex energy. The Green function $G(\boldsymbol{r},\boldsymbol{r}';z)$ is an analytic function of z with the exception of poles and/or branch cuts on the real energy axis. Within the ASA, the Green function for a closely packed solid can be written in the form [15,19,20]

$$\begin{aligned}G(\boldsymbol{r}+\boldsymbol{R},\boldsymbol{r}'+\boldsymbol{R}';z) \;=\; &-\,\delta_{\boldsymbol{R}\boldsymbol{R}'}\;\sum_{L}\;\varphi_{\boldsymbol{R}L}(\boldsymbol{r}^{<},z)\;\tilde{\varphi}_{\boldsymbol{R}L}(\boldsymbol{r}^{>},z)\\ &+\sum_{LL'}\varphi_{\boldsymbol{R}L}(\boldsymbol{r},z)\,G_{\boldsymbol{R}L,\boldsymbol{R}'L'}(z)\,\varphi_{\boldsymbol{R}'L'}(\boldsymbol{r}',z)\;.\end{aligned} \tag{2}$$

Here $\boldsymbol{R},\boldsymbol{R}'$ denote the lattice points (centers of the atomic spheres), L,L' are the angular momentum indices ($L=(\ell,m)$), the variables $\boldsymbol{r},\boldsymbol{r}'$ refer to positions of points inside the individual atomic spheres, and the symbol $\boldsymbol{r}^{<}$ ($\boldsymbol{r}^{>}$) denotes that of the vectors $\boldsymbol{r},\boldsymbol{r}'$ with the smaller (larger) modulus. The functions $\varphi_{\boldsymbol{R}L}(\boldsymbol{r},z)$ and $\tilde{\varphi}_{\boldsymbol{R}L}(\boldsymbol{r},z)$ are defined by

$$\varphi_{\boldsymbol{R}L}(\boldsymbol{r},z)=\varphi_{\boldsymbol{R}\ell}(r,z)\,Y_L(\hat{\boldsymbol{r}})\;,\qquad \tilde{\varphi}_{\boldsymbol{R}L}(\boldsymbol{r},z)=\tilde{\varphi}_{\boldsymbol{R}\ell}(r,z)\,Y_L(\hat{\boldsymbol{r}})\;, \tag{3}$$

where $r=|\boldsymbol{r}|$, $\hat{\boldsymbol{r}}=\boldsymbol{r}/r$, and $Y_L(\hat{\boldsymbol{r}})$ denotes the real spherical harmonics. The radial amplitudes $\varphi_{\boldsymbol{R}\ell}(r,z)$ and $\tilde{\varphi}_{\boldsymbol{R}\ell}(r,z)$ are respectively regular and irregular solutions of the radial Schrödinger equation for the $\boldsymbol{R}$-th atomic sphere of radius $s_{\boldsymbol{R}}$ and for the complex energy z. The regular solution is normalized to unity,

$$\int_0^{s_{\boldsymbol{R}}}\varphi^2_{\boldsymbol{R}\ell}(r,z)\;r^2\;dr\;=\;1\;, \tag{4}$$

while the irregular solution is unambiguously specified by a smooth matching at the sphere boundary ($r=s_{\boldsymbol{R}}$) to the energy derivative of the regular solution $\dot{\varphi}_{\boldsymbol{R}\ell}(r,z)$ (an overdot means energy derivative).

The Green function matrix $G_{\boldsymbol{R}L,\boldsymbol{R}'L'}(z)$ in (2) will be referred to as the physical Green function. It is given in terms of the potential functions $P^0_{\boldsymbol{R}\ell}(z)$ and the canonical structure constants $S^0_{\boldsymbol{R}L,\boldsymbol{R}'L'}$ by

$$G_{\boldsymbol{R}L,\boldsymbol{R}'L'}(z)\;=\;\lambda^0_{\boldsymbol{R}\ell}(z)\;\delta_{\boldsymbol{R}L,\boldsymbol{R}'L'}\;+\;\mu^0_{\boldsymbol{R}\ell}(z)\;g^0_{\boldsymbol{R}L,\boldsymbol{R}'L'}(z)\;\mu^0_{\boldsymbol{R}'\ell'}(z)\;, \tag{5}$$

where the quantities on the r.h.s. are defined as

$$\begin{aligned}\mu^0_{\boldsymbol{R}\ell}(z)\;&=\;\sqrt{\dot{P}^0_{\boldsymbol{R}\ell}(z)}\;,\qquad &\lambda^0_{\boldsymbol{R}\ell}(z)\;&=\;-\,\frac{1}{2}\,\frac{\ddot{P}^0_{\boldsymbol{R}\ell}(z)}{\dot{P}^0_{\boldsymbol{R}\ell}(z)}\;,\\ g^0_{\boldsymbol{R}L,\boldsymbol{R}'L'}(z)\;&=\;\Big\{\big[P^0(z)-S^0\big]^{-1}\Big\}_{\boldsymbol{R}L,\boldsymbol{R}'L'}\;.\end{aligned} \tag{6}$$

In the last equation, the symbol $P^0(z)$ stands for a diagonal matrix of potential functions, $P^0_{\boldsymbol{R}L,\boldsymbol{R}'L'}(z) = P^0_{\boldsymbol{R}\ell}(z)\,\delta_{\boldsymbol{R}L,\boldsymbol{R}'L'}$. The matrix $g^0_{\boldsymbol{R}L,\boldsymbol{R}'L'}(z)$ will be referred to as the auxiliary (or KKR-ASA) Green function. The superscript 0 of all quantities in (5, 6) denotes the canonical LMTO representation. The physical and auxiliary Green functions are connected by a trivial relation (5), the former one is directly related to the Green function in real space (2), the latter one is of a simpler form and thus better suited for numerical applications.

Let us now summarize the most important relations involved in the TB-LMTO theory [16,17]. The superscript α marks the corresponding representation specified by the screening constants $\alpha_{\boldsymbol{R}\ell}$ (the trivial choice $\alpha_{\boldsymbol{R}\ell} = 0$ corresponds to the canonical representation). The transformations of the screened potential functions $P^\alpha_{\boldsymbol{R}\ell}(z)$ and the screened structure constants $S^\alpha_{\boldsymbol{R}L,\boldsymbol{R}'L'}$ from a particular representation α to some other representation β (specified by a different set of the screening constants $\beta_{\boldsymbol{R}\ell}$) are given by

$$\begin{aligned} P^\beta_{\boldsymbol{R}\ell}(z) &= P^\alpha_{\boldsymbol{R}\ell}(z)\,[\,1 + (\alpha_{\boldsymbol{R}\ell} - \beta_{\boldsymbol{R}\ell})\,P^\alpha_{\boldsymbol{R}\ell}(z)\,]^{-1}\ , \\ S^\beta_{\boldsymbol{R}L,\boldsymbol{R}'L'} &= \Big\{ S^\alpha\,[\,1 + (\alpha - \beta)\,S^\alpha\,]^{-1} \Big\}_{\boldsymbol{R}L,\boldsymbol{R}'L'}\ . \end{aligned} \tag{7}$$

These relations serve simultaneously as definitions of the screened quantities from the canonical ones $\big(P^0(z), S^0\big)$. The second equation is written in a matrix notation with α, β being diagonal matrices of the form $\alpha_{\boldsymbol{R}L,\boldsymbol{R}'L'} = \alpha_{\boldsymbol{R}\ell}\delta_{\boldsymbol{R}L,\boldsymbol{R}'L'}$. In analogy to (6), we define

$$\begin{aligned} \mu^\alpha_{\boldsymbol{R}\ell}(z) &= \sqrt{\dot{P}^\alpha_{\boldsymbol{R}\ell}(z)}\ , \qquad & \lambda^\alpha_{\boldsymbol{R}\ell}(z) &= -\,\frac{1}{2}\,\frac{\ddot{P}^\alpha_{\boldsymbol{R}\ell}(z)}{\dot{P}^\alpha_{\boldsymbol{R}\ell}(z)}\ , \\ g^\alpha_{\boldsymbol{R}L,\boldsymbol{R}'L'}(z) &= \Big\{ [P^\alpha(z) - S^\alpha]^{-1} \Big\}_{\boldsymbol{R}L,\boldsymbol{R}'L'}\ . \end{aligned} \tag{8}$$

As a consequence, one can prove two important relations, namely

$$G_{\boldsymbol{R}L,\boldsymbol{R}'L'}(z) = \lambda^\alpha_{\boldsymbol{R}\ell}(z)\,\delta_{\boldsymbol{R}L,\boldsymbol{R}'L'} + \mu^\alpha_{\boldsymbol{R}\ell}(z)\,g^\alpha_{\boldsymbol{R}L,\boldsymbol{R}'L'}(z)\,\mu^\alpha_{\boldsymbol{R}'\ell'}(z)\ , \tag{9}$$

and

$$\begin{aligned} g^\beta_{\boldsymbol{R}L,\boldsymbol{R}'L'}(z) &= (\beta_{\boldsymbol{R}\ell} - \alpha_{\boldsymbol{R}\ell})\,\frac{P^\alpha_{\boldsymbol{R}\ell}(z)}{P^\beta_{\boldsymbol{R}\ell}(z)}\,\delta_{\boldsymbol{R}L,\boldsymbol{R}'L'} \\ &\quad + \frac{P^\alpha_{\boldsymbol{R}\ell}(z)}{P^\beta_{\boldsymbol{R}\ell}(z)}\,g^\alpha_{\boldsymbol{R}L,\boldsymbol{R}'L'}(z)\,\frac{P^\alpha_{\boldsymbol{R}'\ell'}(z)}{P^\beta_{\boldsymbol{R}'\ell'}(z)}\ . \end{aligned} \tag{10}$$

The first relation (9) implies that the physical Green function is invariant with respect to the choice of the screening constants $\alpha_{\boldsymbol{R}\ell}$, cf. (5). The second relation (10) means that the auxiliary Green functions in different representations are related to each other by a simple rescaling. Let us note that the first term on the r.h.s. of (9) does not contribute to calculated physical quantities in most cases. However, its presence is inevitable for correct analytic properties of the Green functions (2, 9) in the complex energy plane.

The only non-trivial step in a calculation of the Green function for a solid is the matrix inversion (8) defining the auxiliary Green function $g^{\alpha}_{\boldsymbol{R}L,\boldsymbol{R}'L'}(z)$. In the case of a bulk solid with three-dimensional translational symmetry, the lattice points $\boldsymbol{R}$ can be expressed in the form $\boldsymbol{R} = \boldsymbol{B} + \boldsymbol{T}$ where $\boldsymbol{B}$ runs over a finite number of the basis vectors while $\boldsymbol{T}$ runs over the translation lattice vectors. The lattice Fourier transformation of the structure constant matrix leads to a $\boldsymbol{k}$-dependent matrix quantity

$$S^{\alpha}_{\boldsymbol{B}L,\boldsymbol{B}'L'}(\boldsymbol{k}) \;=\; \sum_{\boldsymbol{T}} \; S^{\alpha}_{\boldsymbol{B}L,(\boldsymbol{B}'+\boldsymbol{T})L'} \;\exp(\mathrm{i}\,\boldsymbol{k}\cdot\boldsymbol{T}) \;, \tag{11}$$

where $\boldsymbol{k}$ denotes a vector from the first Brillouin zone (BZ). The lattice Fourier transform of the auxiliary Green function, $g^{\alpha}_{\boldsymbol{B}L,\boldsymbol{B}'L'}(\boldsymbol{k},z)$, is given by the inverse of a finite-dimensional matrix:

$$g^{\alpha}_{\boldsymbol{B}L,\boldsymbol{B}'L'}(\boldsymbol{k},z) \;=\; \left\{[P^{\alpha}(z) - S^{\alpha}(\boldsymbol{k})]^{-1}\right\}_{\boldsymbol{B}L,\boldsymbol{B}'L'} \;, \tag{12}$$

where $P^{\alpha}(z)$ denotes a diagonal matrix of the potential functions of the inequivalent atoms, $P^{\alpha}_{\boldsymbol{B}L,\boldsymbol{B}'L'}(z) = P^{\alpha}_{\boldsymbol{B}\ell}(z)\,\delta_{\boldsymbol{B}L,\boldsymbol{B}'L'}$. The inverse Fourier transformation (a BZ-integration) yields then all elements of the auxiliary Green function as

$$g^{\alpha}_{\boldsymbol{B}L,(\boldsymbol{B}'+\boldsymbol{T})L'}(z) \;=\; \frac{1}{N}\;\sum_{\boldsymbol{k}}\; g^{\alpha}_{\boldsymbol{B}L,\boldsymbol{B}'L'}(\boldsymbol{k},z)\;\exp(-\mathrm{i}\,\boldsymbol{k}\cdot\boldsymbol{T}) \;, \tag{13}$$

where N is the number of cells in a large, but finite crystal with periodic boundary conditions.

Further, let us mention the link between the Green functions and the standard LMTO theory. By using parametrized forms of the potential functions $P^{\alpha}_{\boldsymbol{R}\ell}(z)$ and the related quantities $\lambda^{\alpha}_{\boldsymbol{R}\ell}(z)$ and $\mu^{\alpha}_{\boldsymbol{R}\ell}(z)$ which are correct up to the second order in a limited energy region, we get

$$\begin{aligned}
P^{\alpha}_{\boldsymbol{R}\ell}(z) \;&=\; [\,\Delta_{\boldsymbol{R}\ell} \;+\; (\gamma_{\boldsymbol{R}\ell} - \alpha_{\boldsymbol{R}\ell})\;(z - C_{\boldsymbol{R}\ell})\,]^{-1}\;\;(z - C_{\boldsymbol{R}\ell}) \;, \\
\mu^{\alpha}_{\boldsymbol{R}\ell}(z) \;&=\; [\,\Delta_{\boldsymbol{R}\ell} \;+\; (\gamma_{\boldsymbol{R}\ell} - \alpha_{\boldsymbol{R}\ell})\;(z - C_{\boldsymbol{R}\ell})\,]^{-1}\;\;\sqrt{\Delta_{\boldsymbol{R}\ell}} \;, \\
\lambda^{\alpha}_{\boldsymbol{R}\ell}(z) \;&=\; [\,\Delta_{\boldsymbol{R}\ell} \;+\; (\gamma_{\boldsymbol{R}\ell} - \alpha_{\boldsymbol{R}\ell})\;(z - C_{\boldsymbol{R}\ell})\,]^{-1}\;\;(\gamma_{\boldsymbol{R}\ell} - \alpha_{\boldsymbol{R}\ell}) \;,
\end{aligned} \tag{14}$$

where $C_{\boldsymbol{R}\ell}$, $\Delta_{\boldsymbol{R}\ell}$ and $\gamma_{\boldsymbol{R}\ell}$ are the LMTO-ASA potential parameters [4,17]. The insertion of (14) with $\alpha_{\boldsymbol{R}\ell} = 0$ into (5, 6) yields (in a matrix notation):

$$G(z) \;=\; (z - H)^{-1} \;, \qquad H \;=\; C \;+\; \sqrt{\Delta}\,S^{0}\left(1 - \gamma\,S^{0}\right)^{-1}\sqrt{\Delta} \;, \tag{15}$$

which means that the physical Green function is the resolvent of the second-order LMTO-ASA Hamiltonian H. It should be noted that the energy linearization of the LMTO method, which leads to (14) and to the Hamiltonian (15), is not of central importance for the Green function techniques discussed here, as they require matrix inversions rather than matrix diagonalizations.

Finally, let us sketch briefly the evaluation of basic physical observables. As a rule, they are directly related to a limit of the one-electron Green function

$G(\boldsymbol{r},\boldsymbol{r}';z)$ with respect to the upper complex halfplane, $z = E + \mathrm{i}0$, where E denotes a real energy variable. At zero temperature, the electronic charge density $\varrho_{\boldsymbol{R}}(\boldsymbol{r})$ inside the $\boldsymbol{R}$-th atomic sphere (with spin index ignored) can be written as

$$\begin{aligned}\varrho_{\boldsymbol{R}}(\boldsymbol{r}) &= -\frac{1}{\pi}\int_{-\infty}^{E_F} \mathrm{Im}\; G(\boldsymbol{r}+\boldsymbol{R},\boldsymbol{r}+\boldsymbol{R};E+\mathrm{i}0)\; dE \\ &= \sum_{LL'}\int_{-\infty}^{E_F} \varphi_{\boldsymbol{R}L}(\boldsymbol{r},E)\; n_{\boldsymbol{R},LL'}(E)\; \varphi_{\boldsymbol{R}L'}(\boldsymbol{r},E)\; dE\;, \end{aligned} \tag{16}$$

where E_F is the Fermi energy. The quantity $n_{\boldsymbol{R},LL'}(E)$ is the local density of states matrix which is given in terms of the site-diagonal block of the physical Green function

$$n_{\boldsymbol{R},LL'}(E) = -\frac{1}{\pi}\;\mathrm{Im}\; G_{\boldsymbol{R}L,\boldsymbol{R}L'}(E+\mathrm{i}0) \tag{17}$$

and which is closely related to $\boldsymbol{R}L$-projected and local densities of states

$$n_{\boldsymbol{R}L}(E) = n_{\boldsymbol{R},LL}(E)\;, \qquad n_{\boldsymbol{R}}(E) = \sum_{L} n_{\boldsymbol{R}L}(E)\;. \tag{18}$$

The total integrated density of states, $N(E)$, can be obtained from (8, 9, 17, 18). In a matrix notation, the result can be written as [21]

$$\begin{aligned} N(E) &= \sum_{\boldsymbol{R}L}\int_{-\infty}^{E} n_{\boldsymbol{R}L}(\varepsilon)\; d\varepsilon \\ &= \frac{1}{\pi}\;\mathrm{Im}\left[\mathrm{Tr}\;\log\; g^{\alpha}(E+\mathrm{i}0) \;+\; \sum_{\boldsymbol{R}L}\log\;\mu^{\alpha}_{\boldsymbol{R}\ell}(E+\mathrm{i}0)\right], \end{aligned} \tag{19}$$

where the symbol Tr means the trace over the composed $\boldsymbol{R}L$-index. Note that it is the auxiliary (KKR-ASA) Green function which appears in the expression for the integrated density of states $N(E)$, in contrast to the physical Green functions entering the densities of states $n_{\boldsymbol{R}}(E)$ and the charge densities $\varrho_{\boldsymbol{R}}(\boldsymbol{r})$. Despite this fact, $N(E)$ (19) is representation-invariant as can be easily shown.

3 The Coherent Potential Approximation

Let us now consider the simplest model of a substitutionally disordered alloy. We assume several components (atomic species) labeled by a superscript Q ($Q = A, B, \dots$) which occupy randomly the sites $\boldsymbol{R}$ of a given rigid lattice with probabilities $c^{Q}_{\boldsymbol{R}}$ satisfying the conditions

$$\sum_{Q} c^{Q}_{\boldsymbol{R}} = 1\;. \tag{20}$$

We neglect completely any correlations of occupations of different sites and assume that the one-electron potential inside the $\boldsymbol{R}$-th atomic sphere (and consequently the related quantities like the potential functions $P^{\alpha}_{\boldsymbol{R}\ell}(z)$) depends solely on the occupation of this site. In order to express this model in a formal way, we introduce the random occupation index $\eta^{Q}_{\boldsymbol{R}}$ which takes on two values: $\eta^{Q}_{\boldsymbol{R}} = 1$ if an atom of the species Q is at the site $\boldsymbol{R}$, and $\eta^{Q}_{\boldsymbol{R}} = 0$ otherwise. Each configuration of the disordered alloy is thus uniquely specified by these occupation indices which obey the following trivial relations:

$$\sum_{Q} \eta^{Q}_{\boldsymbol{R}} \;=\; 1 \;, \qquad \eta^{Q}_{\boldsymbol{R}}\, \eta^{Q'}_{\boldsymbol{R}} \;=\; \eta^{Q}_{\boldsymbol{R}}\, \delta^{QQ'} \;, \tag{21}$$

which reflect the fact that a given site $\boldsymbol{R}$ cannot be empty or occupied by two different species simultaneously. Let us denote the configurational average of an arbitrary quantity as $\langle \ldots \rangle$, then we get

$$\left\langle \eta^{Q}_{\boldsymbol{R}} \right\rangle \;=\; c^{Q}_{\boldsymbol{R}} \;, \quad \left\langle \eta^{Q}_{\boldsymbol{R}}\, \eta^{Q'}_{\boldsymbol{R}'} \right\rangle \;=\; c^{Q}_{\boldsymbol{R}}\, \delta_{\boldsymbol{R}\boldsymbol{R}'}\, \delta^{QQ'} \;+\; c^{Q}_{\boldsymbol{R}}\, c^{Q'}_{\boldsymbol{R}'}\, (1 - \delta_{\boldsymbol{R}\boldsymbol{R}'}) \;, \tag{22}$$

where the second equation expresses the absence of correlations of the site occupations. The random potential functions $P^{\alpha}_{\boldsymbol{R}\ell}(z)$ can be then written in a form

$$P^{\alpha}_{\boldsymbol{R}\ell}(z) \;=\; \sum_{Q} \eta^{Q}_{\boldsymbol{R}}\, P^{\alpha,Q}_{\boldsymbol{R}\ell}(z) \;, \tag{23}$$

where $P^{\alpha,Q}_{\boldsymbol{R}\ell}(z)$ denotes the non-random potential function of the atom Q occupying the site $\boldsymbol{R}$. Equation (23) represents an important assumption of the model; analogous relations are valid between the random quantities $\lambda^{\alpha}_{\boldsymbol{R}\ell}(z)$, $\mu^{\alpha}_{\boldsymbol{R}\ell}(z)$ (8) and their Q-dependent non-random counterparts $\lambda^{\alpha,Q}_{\boldsymbol{R}\ell}(z)$, $\mu^{\alpha,Q}_{\boldsymbol{R}\ell}(z)$. Let us further assume that the screening constants $\alpha_{\boldsymbol{R}\ell}$ are non-random (configuration-independent). This implies that the structure constant matrix $S^{\alpha}_{\boldsymbol{R}L,\boldsymbol{R}'L'}$ is non-random. The basic problem is an (approximate) configurational averaging of the various one-electron quantities introduced in Sect. 2. In the following, we use a simplified notation with omitted angular momentum indices L, L' so that matrix quantities $X_{\boldsymbol{R}L,\boldsymbol{R}'L'}$ will be abbreviated as $X_{\boldsymbol{R},\boldsymbol{R}'}$ (e.g., $X = S^{\alpha}, g^{\alpha}(z)$), while local (site-diagonal) quantities $W_{\boldsymbol{R},LL'}$ will be abbreviated by $W_{\boldsymbol{R}}$ (e.g., $W = P^{\alpha}(z), \lambda^{\alpha}(z), \mu^{\alpha}(z)$).

We start with the auxiliary Green function $g^{\alpha}_{\boldsymbol{R},\boldsymbol{R}'}(z)$. Its configurational average $\bar{g}^{\alpha}_{\boldsymbol{R},\boldsymbol{R}'}(z)$ can be formally written in a form (cf. (8))

$$\left\langle g^{\alpha}_{\boldsymbol{R},\boldsymbol{R}'}(z) \right\rangle \;=\; \bar{g}^{\alpha}_{\boldsymbol{R},\boldsymbol{R}'}(z) \;=\; \left\{ [\mathcal{P}^{\alpha}(z) - S^{\alpha}]^{-1} \right\}_{\boldsymbol{R},\boldsymbol{R}'} \tag{24}$$

which is nothing but an implicit definition of a non-random matrix quantity $\mathcal{P}^{\alpha}_{\boldsymbol{R},\boldsymbol{R}'}(z)$ – the so-called coherent potential function. The complete knowledge of the latter is equivalent to an exact configurational averaging in (24). Approximate alloy theories like the virtual crystal approximation, the average t-matrix

approximation, and the single-site CPA are based on the neglect of all site non-diagonal blocks of $\mathcal{P}^{\alpha}_{\boldsymbol{R},\boldsymbol{R}'}(z)$:

$$\mathcal{P}^{\alpha}_{\boldsymbol{R},\boldsymbol{R}'}(z) \;=\; \mathcal{P}^{\alpha}_{\boldsymbol{R}}(z)\,\delta_{\boldsymbol{R}\boldsymbol{R}'}\;. \tag{25}$$

This assumption leads to a natural interpretation of the coherent potential functions: $\mathcal{P}^{\alpha}_{\boldsymbol{R},LL'}(z)$ describes the scattering properties of an effective atom at the lattice site $\boldsymbol{R}$. The average Green function (24) corresponds then to a non-random solid formed by the effective atoms placed at the rigid lattice sites.

There are several ways of introducing the single-site CPA [2,7,8]. Here we present the approach of [14,15]. The unknown coherent potential functions $\mathcal{P}^{\alpha}_{\boldsymbol{R}}(z)$ are determined in the following manner. Besides the solid with the effective atoms at all lattice sites, we consider a case with a particular site $\boldsymbol{R}$ occupied by a specified component Q while all other sites are occupied by the effective atoms. The auxiliary Green function in the former case is $\bar{g}^{\alpha}(z)$ (24), whereas that in the latter case will be denoted by $\bar{g}^{\alpha,(\boldsymbol{R}Q)}(z)$. Since the two systems differ only by a perturbation $P^{\alpha,Q}_{\boldsymbol{R}}(z) - \mathcal{P}^{\alpha}_{\boldsymbol{R}}(z)$ which is localized on a single site, the two Green functions are related by

$$\bar{g}^{\alpha,(\boldsymbol{R}Q)}_{\boldsymbol{R}',\boldsymbol{R}''}(z) \;=\; \bar{g}^{\alpha}_{\boldsymbol{R}',\boldsymbol{R}''}(z) \;-\; \bar{g}^{\alpha}_{\boldsymbol{R}',\boldsymbol{R}}(z)\; t^{\alpha,Q}_{\boldsymbol{R}}(z)\; \bar{g}^{\alpha}_{\boldsymbol{R},\boldsymbol{R}''}(z)\;. \tag{26}$$

The quantity $t^{\alpha,Q}_{\boldsymbol{R},LL'}(z)$ is the single-site t-matrix describing the scattering due to a Q-impurity in an effective medium formed by the effective atoms. It is explicitly given by

$$\begin{aligned} t^{\alpha,Q}_{\boldsymbol{R}}(z) \;&=\; f^{\alpha,Q}_{\boldsymbol{R}}(z)\left[P^{\alpha,Q}_{\boldsymbol{R}}(z) - \mathcal{P}^{\alpha}_{\boldsymbol{R}}(z)\right] \\ &=\; \left[P^{\alpha,Q}_{\boldsymbol{R}}(z) - \mathcal{P}^{\alpha}_{\boldsymbol{R}}(z)\right] \tilde{f}^{\alpha,Q}_{\boldsymbol{R}}(z)\;, \end{aligned} \tag{27}$$

where

$$\begin{aligned} f^{\alpha,Q}_{\boldsymbol{R}}(z) \;&=\; \left\{1 \;+\; \left[P^{\alpha,Q}_{\boldsymbol{R}}(z) - \mathcal{P}^{\alpha}_{\boldsymbol{R}}(z)\right] \bar{g}^{\alpha}_{\boldsymbol{R},\boldsymbol{R}}(z)\right\}^{-1}\;, \\ \tilde{f}^{\alpha,Q}_{\boldsymbol{R}}(z) \;&=\; \left\{1 \;+\; \bar{g}^{\alpha}_{\boldsymbol{R},\boldsymbol{R}}(z)\left[P^{\alpha,Q}_{\boldsymbol{R}}(z) - \mathcal{P}^{\alpha}_{\boldsymbol{R}}(z)\right]\right\}^{-1}\;. \end{aligned} \tag{28}$$

The CPA condition for the coherent potential functions can be now formulated as

$$\sum_{Q} c^{Q}_{\boldsymbol{R}}\; \bar{g}^{\alpha,(\boldsymbol{R}Q)}_{\boldsymbol{R}',\boldsymbol{R}''}(z) \;=\; \bar{g}^{\alpha}_{\boldsymbol{R}',\boldsymbol{R}''}(z)\;, \tag{29}$$

which expresses the equivalence of the average Green function $\bar{g}^{\alpha}(z)$ and a concentration-weighted sum of the Green functions $\bar{g}^{\alpha,(\boldsymbol{R}Q)}(z)$, see Fig. 1.

As it is obvious from (26), the relation (29) is equivalent to

$$\sum_{Q} c^{Q}_{\boldsymbol{R}}\; t^{\alpha,Q}_{\boldsymbol{R}}(z) \;=\; 0\;, \tag{30}$$

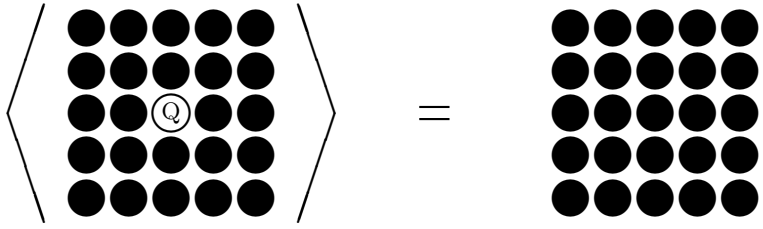

Fig. 1. The selfconsistency condition of the CPA

which is a condition for vanishing average scattering from the Q-impurities ($Q = A, B, \dots$) embedded in the effective medium.

Equation (30) represents the standard form of the CPA selfconsistency condition [2,7,8] which specifies implicitly the coherent potential functions $\mathcal{P}^{\alpha}_{\boldsymbol{R}}(z)$. It should be noted that $\mathcal{P}^{\alpha}_{\boldsymbol{R},LL'}(z)$ are in general non-diagonal matrices in the L, L' indices, in contrast to the potential functions of the individual components ($P^{\alpha,Q}_{\boldsymbol{R},LL'}(z) = P^{\alpha,Q}_{\boldsymbol{R}\ell}(z)\,\delta_{LL'}$). The CPA condition (30) has to be solved for all sites simultaneously as the single-site t-matrices (27, 28) involve the site-diagonal blocks of the full matrix inversion defining the average Green function (24). In practice, this can be done only if the whole lattice can be represented by a finite number of inequivalent sites. In the case of a bulk alloy with a crystal lattice and with a possible long-range order, the lattice sites can be written as $\boldsymbol{R} = \boldsymbol{B} + \boldsymbol{T}$ (see the text before (11)), where $\boldsymbol{B}$ labels the inequivalent sites, and the alloy is specified by the concentrations $c^{Q}_{\boldsymbol{B}}$ and the component-dependent potential functions $P^{\alpha,Q}_{\boldsymbol{B}\ell}(z)$. As a consequence, the coherent potential functions for all lattice sites reduce to a finite set of matrix quantities $\mathcal{P}^{\alpha}_{\boldsymbol{B},LL'}(z)$. In analogy to (12), the lattice Fourier transform of the average auxiliary Green function is given by

$$\bar{g}^{\alpha}_{\boldsymbol{B}L,\boldsymbol{B}'L'}(\boldsymbol{k},z) \;=\; \left\{[\mathcal{P}^{\alpha}(z) - S^{\alpha}(\boldsymbol{k})]^{-1}\right\}_{\boldsymbol{B}L,\boldsymbol{B}'L'} \;, \tag{31}$$

where the matrix $S^{\alpha}(\boldsymbol{k})$ is given by (11) and $\mathcal{P}^{\alpha}(z)$ denotes a matrix of the coherent potential functions of the inequivalent sites, $\mathcal{P}^{\alpha}_{\boldsymbol{B}L,\boldsymbol{B}'L'}(z) = \mathcal{P}^{\alpha}_{\boldsymbol{B},LL'}(z)\,\delta_{\boldsymbol{B}\boldsymbol{B}'}$. A subsequent BZ-integration yields the elements of the average auxiliary Green function (cf. (13))

$$\bar{g}^{\alpha}_{\boldsymbol{B}L,(\boldsymbol{B}'+\boldsymbol{T})L'}(z) \;=\; \frac{1}{N}\,\sum_{\boldsymbol{k}}\,\bar{g}^{\alpha}_{\boldsymbol{B}L,\boldsymbol{B}'L'}(\boldsymbol{k},z)\;\exp(-\mathrm{i}\,\boldsymbol{k}\cdot\boldsymbol{T})\;. \tag{32}$$

It should be noted that only the site-diagonal blocks ($\boldsymbol{B} = \boldsymbol{B}'$, $\boldsymbol{T} = \boldsymbol{0}$) of $\bar{g}^{\alpha}(z)$ enter the CPA selfconsistency condition (30). The appearance of $\boldsymbol{k}$-dependent quantities in the description of random substitutional alloys reflects a well-known fact that the configurational averaging restores the translational symmetry (absent for individual configurations of the alloy).

Despite the fact that the CPA condition (30) represents a set of coupled nonlinear equations for the complex matrix quantities $\mathcal{P}^{\alpha}_{\boldsymbol{R},LL'}(z)$, general theorems

guarantee the existence of its unique solution which possesses the so-called Herglotz property. The latter means that (i) the coherent potential functions are analytic functions of z outside the real energy axis, and (ii) the imaginary part of the matrix $\mathcal{P}^{\alpha}_{\boldsymbol{R}}(z)$ is positive (negative) definite for $\mathrm{Im}\, z > 0$ ($\mathrm{Im}\, z < 0$).

3.1 Site-Diagonal Quantities

The calculation of average local quantities like the charge densities (16) or the local densities of states (18) requires a knowledge of additional quantities besides the site-diagonal blocks of the average Green function (24). One introduces so-called conditionally averaged local auxiliary Green functions $\bar{g}^{\alpha,Q}_{\boldsymbol{R},\boldsymbol{R}}(z)$ defined by

$$\bar{g}^{\alpha,Q}_{\boldsymbol{R},\boldsymbol{R}}(z) \;=\; \left(c^{Q}_{\boldsymbol{R}}\right)^{-1} \left\langle \eta^{Q}_{\boldsymbol{R}}\, g^{\alpha}_{\boldsymbol{R},\boldsymbol{R}}(z) \right\rangle \;. \tag{33}$$

This quantity corresponds to the site-diagonal $(\boldsymbol{R},\boldsymbol{R})$-th block of the Green function averaged under the condition that the site $\boldsymbol{R}$ is occupied by the atomic species Q. Within the CPA, $\bar{g}^{\alpha,Q}_{\boldsymbol{R},\boldsymbol{R}}(z)$ is equal to the $(\boldsymbol{R},\boldsymbol{R})$-th block of the Green function $\bar{g}^{\alpha,(\boldsymbol{R}Q)}(z)$ (26) corresponding to an $\boldsymbol{R}Q$-impurity in the effective medium:

$$\bar{g}^{\alpha,Q}_{\boldsymbol{R},\boldsymbol{R}}(z) \;=\; \bar{g}^{\alpha}_{\boldsymbol{R},\boldsymbol{R}}(z) \;-\; \bar{g}^{\alpha}_{\boldsymbol{R},\boldsymbol{R}}(z)\, t^{\alpha,Q}_{\boldsymbol{R}}(z)\, \bar{g}^{\alpha}_{\boldsymbol{R},\boldsymbol{R}}(z) \;. \tag{34}$$

An equivalent form of this result can be obtained with the help of (28):

$$\bar{g}^{\alpha,Q}_{\boldsymbol{R},\boldsymbol{R}}(z) \;=\; \bar{g}^{\alpha}_{\boldsymbol{R},\boldsymbol{R}}(z)\, f^{\alpha,Q}_{\boldsymbol{R}}(z) \;=\; \tilde{f}^{\alpha,Q}_{\boldsymbol{R}}(z)\, \bar{g}^{\alpha}_{\boldsymbol{R},\boldsymbol{R}}(z) \;. \tag{35}$$

It follows immediately from (34, 35) that the CPA selfconsistency condition (30) can be expressed in two other forms, namely,

$$\sum_{Q} c^{Q}_{\boldsymbol{R}}\, \bar{g}^{\alpha,Q}_{\boldsymbol{R},\boldsymbol{R}}(z) \;=\; \bar{g}^{\alpha}_{\boldsymbol{R},\boldsymbol{R}}(z) \;, \tag{36}$$

and

$$\sum_{Q} c^{Q}_{\boldsymbol{R}}\, f^{\alpha,Q}_{\boldsymbol{R}}(z) \;=\; \sum_{Q} c^{Q}_{\boldsymbol{R}}\, \tilde{f}^{\alpha,Q}_{\boldsymbol{R}}(z) \;=\; 1 \;. \tag{37}$$

The first of them can be easily interpreted: the concentration-weighted average of the Q-dependent conditionally averaged local Green functions is equal to the site-diagonal block of the average Green function.

Let us now discuss the averaging of local observables. We define the conditionally averaged local physical Green functions $\bar{G}^{Q}_{\boldsymbol{R},\boldsymbol{R}}(z)$ as

$$\bar{G}^{Q}_{\boldsymbol{R},\boldsymbol{R}}(z) \;=\; \left(c^{Q}_{\boldsymbol{R}}\right)^{-1} \left\langle \eta^{Q}_{\boldsymbol{R}}\, G_{\boldsymbol{R},\boldsymbol{R}}(z) \right\rangle \;. \tag{38}$$

Taking into account (9) and the simple configuration dependence of $P^{\alpha}_{\boldsymbol{R}\ell}(z)$, $\lambda^{\alpha}_{\boldsymbol{R}\ell}(z)$, and $\mu^{\alpha}_{\boldsymbol{R}\ell}(z)$ (23), we obtain finally

$$\bar{G}^{Q}_{\boldsymbol{R}L,\boldsymbol{R}L'}(z) \;=\; \lambda^{\alpha,Q}_{\boldsymbol{R}\ell}(z)\;\delta_{LL'} \;+\; \mu^{\alpha,Q}_{\boldsymbol{R}\ell}(z)\;\bar{g}^{\alpha,Q}_{\boldsymbol{R}L,\boldsymbol{R}L'}(z)\;\mu^{\alpha,Q}_{\boldsymbol{R}\ell'}(z)\;. \tag{39}$$

The expressions (16, 17, 18) can be modified to get the Q-resolved average quantities: the local density of states matrix

$$n^{Q}_{\boldsymbol{R},LL'}(E) \;=\; -\;\frac{1}{\pi}\;\mathrm{Im}\;\bar{G}^{Q}_{\boldsymbol{R}L,\boldsymbol{R}L'}(E+\mathrm{i}0)\;, \tag{40}$$

the densities of states

$$n^{Q}_{\boldsymbol{R}L}(E) \;=\; n^{Q}_{\boldsymbol{R},LL}(E)\;, \qquad\qquad n^{Q}_{\boldsymbol{R}}(E) \;=\; \sum_{L}\; n^{Q}_{\boldsymbol{R}L}(E)\;, \tag{41}$$

and the charge densities

$$\varrho^{Q}_{\boldsymbol{R}}(\boldsymbol{r}) \;=\; \sum_{LL'}\;\int_{-\infty}^{E_F}\;\varphi^{Q}_{\boldsymbol{R}L}(\boldsymbol{r},E)\;n^{Q}_{\boldsymbol{R},LL'}(E)\;\varphi^{Q}_{\boldsymbol{R}L'}(\boldsymbol{r},E)\;dE\;. \tag{42}$$

One can also define average local quantities as concentration-weighted sums of the corresponding Q-resolved quantities, e.g.,

$$n_{\boldsymbol{R}L}(E) \;=\; \sum_{Q}\;c^{Q}_{\boldsymbol{R}}\,n^{Q}_{\boldsymbol{R}L}(E)\;, \qquad\qquad n_{\boldsymbol{R}}(E) \;=\; \sum_{Q}\;c^{Q}_{\boldsymbol{R}}\,n^{Q}_{\boldsymbol{R}}(E)\;, \tag{43}$$

which define average densities of states.

The CPA expression for the configuration average of the total integrated density of states $N(E)$ is not a simple generalization of (19). The final result is given by [2,14,22]

$$\begin{aligned} N(E) \;=\; \frac{1}{\pi}\;\mathrm{Im}\;\Bigg[\;&\mathrm{Tr}\;\log\;\bar{g}^{\alpha}(E+\mathrm{i}0) \;+\; \sum_{\boldsymbol{R}Q}\;c^{Q}_{\boldsymbol{R}}\;\mathrm{tr}\;\log\;f^{\alpha,Q}_{\boldsymbol{R}}(E+\mathrm{i}0) \\ &+\; \sum_{\boldsymbol{R}QL}\;c^{Q}_{\boldsymbol{R}}\;\log\;\mu^{\alpha,Q}_{\boldsymbol{R}\ell}(E+\mathrm{i}0)\;\Bigg]\;, \end{aligned} \tag{44}$$

where the symbol tr means the trace over the angular momentum index L. Let us mention an important variational property of $N(E)$ (44), which is a direct consequence of the CPA selfconsistency [22]: $N(E)$ is stationary with respect to variations of the coherent potential functions $\delta\mathcal{P}^{\alpha}_{\boldsymbol{R}}(z)$. This property makes the CPA an excellent starting point for studies of alloy energetics within the generalized perturbation method [23,24].

In numerical implementations of the CPA as well as of other Green function techniques, complex energies are indispensable to obtain the limiting values at the real energy axis, cf. (40, 44). A useful approach to get the necessary limits $F(E+\mathrm{i}0)$ of a complex function $F(z)$ analytic in the upper halfplane is based on

a relatively easy evaluation of the function $F(z)$ for $\mathrm{Im}\, z > 0$ and a subsequent analytic continuation to the real axis [25]. This procedure is justified by the Riemann-Cauchy relations and it employs truncated Taylor expansions of the function $F(z)$. Suppose that $F(z)$ has to be evaluated for real energies on a dense equidistant mesh of energy points $E_n = E_0 + nh$, where h is an energy step and $n = 0, 1, \ldots, N$. Let us consider a discrete set of complex energy points

$$z_{n,m} \;=\; E_0 \;+\; n\,h \;+\; \mathrm{i}\,m\,h \;, \tag{45}$$

where $m = 0, 1, \ldots, M$, and let us abbreviate $F_{n,m} = F(z_{n,m})$. The first step of a continuation procedure is the calculation of $F_{n,M}$ for $-M \le n \le N + M$, i.e., for complex energies along a line parallel to the real axis. In each of the M following steps, the values of $F_{n,m}$ with m reduced by one are obtained from all previously calculated values. The simplest examples are given by relations:

$$F_{n,m-1} \;=\; 2\,F_{n,m} \;+\; \frac{-1+\mathrm{i}}{2}\,F_{n-1,m} \;+\; \frac{-1-\mathrm{i}}{2}\,F_{n+1,m} \;, \tag{46}$$

which is based on a quadratic Taylor expansion, and

$$F_{n,m-1} \;=\; F_{n,m} \;+\; \frac{\mathrm{i}}{2}\,F_{n-1,m} \;-\; \frac{\mathrm{i}}{2}\,F_{n+1,m} \;, \tag{47}$$

which is based on a repeated linear Taylor expansion. There are many modifications of this procedure which employ higher-order expansions [15,25]. However, only the linear continuation (47) yields always strictly non-negative densities of states and the Bloch spectral functions. Typically, an energy increment of $h \sim 5$ mRy and $M \sim 2$ to 5 lead to a sufficiently large $\mathrm{Im}\, z$ for an initial calculation of $F(z)$. The continuation to the real axis according to (46, 47) represents then a negligible computational effort.

An example of average densities of states is presented in Fig. 2 for a spin-polarized random bcc $Fe_{0.7}V_{0.3}$ alloy. Due to the antiparallel magnetic moments of the Fe and V atoms, the spin-up electrons feel a much stronger disorder than the spin-down electrons. The different degree of disorder is nicely reflected in the shapes of the local densities of states: the spin-down densities for both components (Fig. 2b) resemble those for the pure elements in the bcc structure whereas the spin-up densities (Fig. 2a) are strongly modified due to alloying. Especially in the latter case, the CPA describes the electronic structure substantially better than other single-site theories (the virtual crystal approximation, the average t-matrix approximation).

3.2 Site Non-Diagonal Quantities

Let us now turn to the physical Green function $G_{\boldsymbol{R},\boldsymbol{R}'}(z)$ and to its configurational average

$$\langle G_{\boldsymbol{R},\boldsymbol{R}'}(z) \rangle \;=\; \bar{G}_{\boldsymbol{R},\boldsymbol{R}'}(z) \;, \tag{48}$$

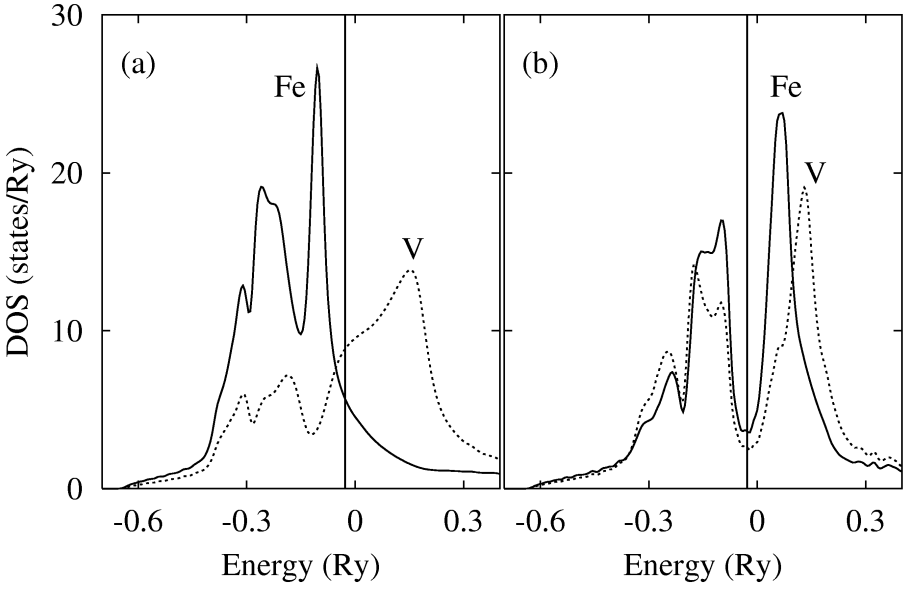

Fig. 2. Spin-polarized local densities of states for Fe (*full lines*) and V (*dotted lines*) atoms in the random bcc $Fe_{0.7}V_{0.3}$ alloy: (**a**) spin-up electrons, (**b**) spin-down electrons. The vertical lines denote the position of the Fermi energy

and let us treat separately its site-diagonal ($\boldsymbol{R} = \boldsymbol{R}'$) and site non-diagonal ($\boldsymbol{R} \neq \boldsymbol{R}'$) blocks. The former are given directly by

$$\bar{G}_{\boldsymbol{R},\boldsymbol{R}}(z) \;=\; \sum_{Q} c^{Q}_{\boldsymbol{R}}\, \bar{G}^{Q}_{\boldsymbol{R},\boldsymbol{R}}(z)\;, \tag{49}$$

where the conditionally averaged blocks $\bar{G}^{Q}_{\boldsymbol{R},\boldsymbol{R}}(z)$ can be expressed according to (39). The site non-diagonal blocks can be rewritten with the help of (9, 23) as

$$\bar{G}_{\boldsymbol{R},\boldsymbol{R}'}(z) \;=\; \sum_{QQ'} \mu^{\alpha,Q}_{\boldsymbol{R}}(z)\, \left\langle \eta^{Q}_{\boldsymbol{R}}\, g^{\alpha}_{\boldsymbol{R},\boldsymbol{R}'}(z)\, \eta^{Q'}_{\boldsymbol{R}'} \right\rangle\, \mu^{\alpha,Q'}_{\boldsymbol{R}'}(z)\;. \tag{50}$$

The configurational average on the r.h.s. of (50) represents (apart from a normalization) a more complicated case of a conditional average: it refers to the site non-diagonal $(\boldsymbol{R}, \boldsymbol{R}')$-th block of the auxiliary Green function averaged under the condition that the two sites $\boldsymbol{R}, \boldsymbol{R}'$ are occupied by the atomic species Q, Q', respectively. The single-site CPA expression for this kind of conditional average is [10,11]

$$\left\langle \eta^{Q}_{\boldsymbol{R}}\, g^{\alpha}_{\boldsymbol{R},\boldsymbol{R}'}(z)\, \eta^{Q'}_{\boldsymbol{R}'} \right\rangle \;=\; c^{Q}_{\boldsymbol{R}}\, \tilde{f}^{\alpha,Q}_{\boldsymbol{R}}(z)\, \bar{g}^{\alpha}_{\boldsymbol{R},\boldsymbol{R}'}(z)\, c^{Q'}_{\boldsymbol{R}'}\, f^{\alpha,Q'}_{\boldsymbol{R}'}(z)\;. \tag{51}$$

Equation (51) can be derived for binary alloys by means of a simple algebraic technique [14] while for the multicomponent case one can use Green functions

in an extended space [2,9]:

$$\hat{g}^{\alpha}_{\boldsymbol{R}QL,\boldsymbol{R}'Q'L'}(z) \;=\; \eta^{Q}_{\boldsymbol{R}}\, g^{\alpha}_{\boldsymbol{R}L,\boldsymbol{R}'L'}(z)\, \eta^{Q'}_{\boldsymbol{R}'} \;. \tag{52}$$

A single-site CPA averaging of (52) yields then the result (51) [2]. The final expression for the average physical Green function follows from (49, 50, 51) and can be compactly written as

$$\begin{aligned} \bar{G}_{\boldsymbol{R},\boldsymbol{R}'}(z) \;&=\; \bar{G}_{\boldsymbol{R},\boldsymbol{R}}(z)\, \delta_{\boldsymbol{R}\boldsymbol{R}'} \;+\; \tilde{\mathcal{M}}^{\alpha}_{\boldsymbol{R}}(z)\, \bar{g}^{\alpha}_{\boldsymbol{R},\boldsymbol{R}'}(z)\, \mathcal{M}^{\alpha}_{\boldsymbol{R}'}(z)\, (1-\delta_{\boldsymbol{R}\boldsymbol{R}'}) \\ &=\; \mathcal{L}^{\alpha}_{\boldsymbol{R}}(z)\, \delta_{\boldsymbol{R}\boldsymbol{R}'} \;+\; \tilde{\mathcal{M}}^{\alpha}_{\boldsymbol{R}}(z)\, \bar{g}^{\alpha}_{\boldsymbol{R},\boldsymbol{R}'}(z)\, \mathcal{M}^{\alpha}_{\boldsymbol{R}'}(z) \;, \end{aligned} \tag{53}$$

where

$$\begin{aligned} \mathcal{M}^{\alpha}_{\boldsymbol{R}}(z) \;&=\; \sum_{Q} c^{Q}_{\boldsymbol{R}}\, f^{\alpha,Q}_{\boldsymbol{R}}(z)\, \mu^{\alpha,Q}_{\boldsymbol{R}}(z) \;, \\ \tilde{\mathcal{M}}^{\alpha}_{\boldsymbol{R}}(z) \;&=\; \sum_{Q} c^{Q}_{\boldsymbol{R}}\, \mu^{\alpha,Q}_{\boldsymbol{R}}(z)\, \tilde{f}^{\alpha,Q}_{\boldsymbol{R}}(z) \;, \end{aligned} \tag{54}$$

and

$$\mathcal{L}^{\alpha}_{\boldsymbol{R}}(z) \;=\; \bar{G}_{\boldsymbol{R},\boldsymbol{R}}(z) \;-\; \tilde{\mathcal{M}}^{\alpha}_{\boldsymbol{R}}(z)\, \bar{g}^{\alpha}_{\boldsymbol{R},\boldsymbol{R}}(z)\, \mathcal{M}^{\alpha}_{\boldsymbol{R}}(z) \;. \tag{55}$$

It should be noted that the final relation between $\bar{G}_{\boldsymbol{R},\boldsymbol{R}'}(z)$ and $\bar{g}^{\alpha}_{\boldsymbol{R},\boldsymbol{R}'}(z)$ (53) bears the same formal structure as (9) for the non-averaged Green functions.

The average physical Green function (53) can be now used to calculate the Bloch spectral functions. Let us consider again the case of a random bulk alloy with a crystal lattice and with a possible long-range order. The lattice sites can be written as $\boldsymbol{R} = \boldsymbol{B} + \boldsymbol{T}$, where $\boldsymbol{B}$ labels the inequivalent sites and $\boldsymbol{T}$ runs over the translation vectors of the configurationally averaged system (see the text near (31, 32)). The Bloch spectral functions are defined in terms of the lattice Fourier transform of $\bar{G}_{\boldsymbol{R},\boldsymbol{R}'}(z)$:

$$\begin{aligned} \mathcal{A}_{\boldsymbol{B}L}(\boldsymbol{k},E) \;&=\; -\,\frac{1}{\pi}\, \mathrm{Im}\, \bar{G}_{\boldsymbol{B}L,\boldsymbol{B}L}(\boldsymbol{k},E+\mathrm{i}0) \;, \\ \mathcal{A}_{\boldsymbol{B}}(\boldsymbol{k},E) \;&=\; \sum_{L} \mathcal{A}_{\boldsymbol{B}L}(\boldsymbol{k},E) \;. \end{aligned} \tag{56}$$

As follows from (53), the lattice Fourier transform of $\bar{G}_{\boldsymbol{R},\boldsymbol{R}'}(z)$ can be reduced to that of $\bar{g}^{\alpha}_{\boldsymbol{R},\boldsymbol{R}'}(z)$ which in turn is given by (31):

$$\begin{aligned} \bar{G}_{\boldsymbol{B}L,\boldsymbol{B}L}(\boldsymbol{k},z) \;=\; \sum_{L'L''} \tilde{\mathcal{M}}^{\alpha}_{\boldsymbol{B},LL'}(z)\, \bar{g}^{\alpha}_{\boldsymbol{B}L',\boldsymbol{B}L''}(\boldsymbol{k},z)\, \mathcal{M}^{\alpha}_{\boldsymbol{B},L''L}(z) \\ +\, \mathcal{L}^{\alpha}_{\boldsymbol{B},LL}(z) \;. \end{aligned} \tag{57}$$

Using (53) and elementary properties of lattice Fourier transformations, one can prove a relation between the Bloch spectral function $\mathcal{A}_{\boldsymbol{B}L}(\boldsymbol{k},E)$ and the corresponding average density of states $n_{\boldsymbol{B}L}(E)$ (43), namely,

$$n_{\boldsymbol{B}L}(E) \;=\; \frac{1}{N} \sum_{\boldsymbol{k}} \mathcal{A}_{\boldsymbol{B}L}(\boldsymbol{k},E) \;. \tag{58}$$

According to this sum rule, the Bloch spectral function reflects the contributions of different parts of the BZ to the resulting density of states of the configurationally averaged system. Let us note that in the case of non-random crystalline solids, the spectral functions for a given fixed $\boldsymbol{k}$-vector reduce to sums of δ-functions located at the corresponding energy eigenvalues. Hence, the concept of the Bloch spectral functions substitutes energy bands in random alloys and can be used, e.g., for a definition of the Fermi surfaces. The latter are based on the $\boldsymbol{k}$-dependence of the spectral functions (56) evaluated at a constant energy ($E = E_F$).

3.3 Transformation Properties of the LMTO-CPA

The physical properties of a non-random system described by the TB-LMTO-ASA method do not depend on the choice of a particular LMTO representation α as expressed by (5, 9). In the context of random alloys, it is of fundamental importance to know whether this feature survives the approximate configuration averaging within the single-site CPA. The answer is positive [15] as will be shown below.

We assume that the representations α, β are specified by non-random screening constants $\alpha_{\boldsymbol{R}\ell}, \beta_{\boldsymbol{R}\ell}$, respectively. For simplicity, we will omit the energy arguments as well as the angular momentum indices L, L'. The transformation of the coherent potential functions is analogous to (7), namely,

$$\mathcal{P}^{\beta}_{\boldsymbol{R}} \;=\; \mathcal{P}^{\alpha}_{\boldsymbol{R}} \,[\, 1 \,+\, (\alpha_{\boldsymbol{R}} - \beta_{\boldsymbol{R}})\, \mathcal{P}^{\alpha}_{\boldsymbol{R}} \,]^{-1} \;. \tag{59}$$

The transformations of the coherent potential functions (59) and of the non-random structure constants (7) lead to the following transformation of the average auxiliary Green functions:

$$\begin{aligned} \bar{g}^{\beta}_{\boldsymbol{R},\boldsymbol{R}'} \;&=\; (\beta_{\boldsymbol{R}} - \alpha_{\boldsymbol{R}})\; \mathcal{P}^{\alpha}_{\boldsymbol{R}} \left(\mathcal{P}^{\beta}_{\boldsymbol{R}}\right)^{-1} \delta_{\boldsymbol{R}\boldsymbol{R}'} \\ &\quad +\; \left(\mathcal{P}^{\beta}_{\boldsymbol{R}}\right)^{-1} \mathcal{P}^{\alpha}_{\boldsymbol{R}}\; \bar{g}^{\alpha}_{\boldsymbol{R},\boldsymbol{R}'}\; \mathcal{P}^{\alpha}_{\boldsymbol{R}'} \left(\mathcal{P}^{\beta}_{\boldsymbol{R}'}\right)^{-1} \end{aligned} \tag{60}$$

which is of the same structure as (10). The transformation of the perturbation related to a single Q-impurity embedded in the effective medium is given by

$$P^{\beta,Q}_{\boldsymbol{R}} - \mathcal{P}^{\beta}_{\boldsymbol{R}} \;=\; P^{\beta,Q}_{\boldsymbol{R}} \left(P^{\alpha,Q}_{\boldsymbol{R}}\right)^{-1} \;\left(P^{\alpha,Q}_{\boldsymbol{R}} - \mathcal{P}^{\alpha}_{\boldsymbol{R}}\right)\; (\mathcal{P}^{\alpha}_{\boldsymbol{R}})^{-1}\; \mathcal{P}^{\beta}_{\boldsymbol{R}} \,, \tag{61}$$

as can be easily derived from (7, 59). The transformation of the quantities (28) can be obtained with the help of (61) and of the site-diagonal blocks of (60). The result is

$$\begin{aligned} f^{\beta,Q}_{\boldsymbol{R}} \;&=\; \mathcal{P}^{\beta}_{\boldsymbol{R}}\; (\mathcal{P}^{\alpha}_{\boldsymbol{R}})^{-1}\; f^{\alpha,Q}_{\boldsymbol{R}}\; P^{\alpha,Q}_{\boldsymbol{R}} \left(P^{\beta,Q}_{\boldsymbol{R}}\right)^{-1} \;, \\ \tilde{f}^{\beta,Q}_{\boldsymbol{R}} \;&=\; \left(P^{\beta,Q}_{\boldsymbol{R}}\right)^{-1} P^{\alpha,Q}_{\boldsymbol{R}}\; \tilde{f}^{\alpha,Q}_{\boldsymbol{R}}\; (\mathcal{P}^{\alpha}_{\boldsymbol{R}})^{-1}\; \mathcal{P}^{\beta}_{\boldsymbol{R}} \,, \end{aligned} \tag{62}$$

which can be combined with (61) to get the transformation of the single-site t-matrices (27):

$$t^{\beta,Q}_{\boldsymbol{R}} \;=\; \mathcal{P}^{\beta}_{\boldsymbol{R}}\,(\mathcal{P}^{\alpha}_{\boldsymbol{R}})^{-1}\;t^{\alpha,Q}_{\boldsymbol{R}}\;(\mathcal{P}^{\alpha}_{\boldsymbol{R}})^{-1}\,\mathcal{P}^{\beta}_{\boldsymbol{R}}\,. \tag{63}$$

An immediate consequence of (63) is the simultaneous validity of the CPA selfconsistency condition (30) in two different LMTO representations. This means that all CPA effective media are mutually equivalent irrespective of the particular LMTO representation used for the formulation and solution of the selfconsistency condition.

The transformations of other quantities can be derived from (59–63). This yields, e.g., for the conditionally averaged local auxiliary Green functions (35) a relation completely analogous to (10):

$$\begin{aligned}\bar{g}^{\beta,Q}_{\boldsymbol{R}L,\boldsymbol{R}L'}(z) \;=\; & (\beta_{\boldsymbol{R}\ell}-\alpha_{\boldsymbol{R}\ell})\,\frac{P^{\alpha,Q}_{\boldsymbol{R}\ell}(z)}{P^{\beta,Q}_{\boldsymbol{R}\ell}(z)}\,\delta_{LL'} \\ & +\,\frac{P^{\alpha,Q}_{\boldsymbol{R}\ell}(z)}{P^{\beta,Q}_{\boldsymbol{R}\ell}(z)}\;\bar{g}^{\alpha,Q}_{\boldsymbol{R}L,\boldsymbol{R}L'}(z)\;\frac{P^{\alpha,Q}_{\boldsymbol{R}\ell'}(z)}{P^{\beta,Q}_{\boldsymbol{R}\ell'}(z)}\,.\end{aligned} \tag{64}$$

One can further show that CPA averages of the physical Green functions (38, 48) remain invariant with respect to different LMTO representations α, which in turn implies the invariance of all physical observables and proves a full compatibility of the single-site CPA with the TB-LMTO method.

3.4 Solution of the CPA Selfconsistency

It should be noted that although the above three forms of the CPA condition (30, 36, 37) are mathematically equivalent, not all of them are suitable for numerical applications. For this purpose we will introduce the so-called coherent interactor $\Omega^{\alpha}_{\boldsymbol{R},LL'}(z)$ [2,9,14] which is a local quantity defined implicitly in terms of the coherent potential function and the site-diagonal block of the average auxiliary Green function as

$$\bar{g}^{\alpha}_{\boldsymbol{R},\boldsymbol{R}}(z) \;=\; [\,\mathcal{P}^{\alpha}_{\boldsymbol{R}}(z) \;-\; \Omega^{\alpha}_{\boldsymbol{R}}(z)\,]^{-1}\;, \tag{65}$$

or, explicitly, as

$$\Omega^{\alpha}_{\boldsymbol{R}}(z) \;=\; \mathcal{P}^{\alpha}_{\boldsymbol{R}}(z) \;-\; \left[\,\bar{g}^{\alpha}_{\boldsymbol{R},\boldsymbol{R}}(z)\,\right]^{-1}\;. \tag{66}$$

The coherent interactor describes the effective coupling of a given site $\boldsymbol{R}$ to all other sites in the system. Using this definition, one can express the conditionally averaged local auxiliary Green function as

$$\bar{g}^{\alpha,Q}_{\boldsymbol{R},\boldsymbol{R}}(z) \;=\; \left[\,P^{\alpha,Q}_{\boldsymbol{R}}(z) \;-\; \Omega^{\alpha}_{\boldsymbol{R}}(z)\,\right]^{-1}\;. \tag{67}$$

In the following, we describe a simple iterative scheme solving the CPA condition (36) using the coherent interactor and (65, 67). We assume that the energy z lies

outside the real energy axis. For brevity, the energy argument z and the orbital indices L, L' will be omitted.

The algorithm starts from an input value $\Omega_{\boldsymbol{R}}^{\alpha,(0)}$ which can be set either to zero or, e.g., to the converged coherent interactor for a neighboring energy argument. For a particular iteration leading from $\Omega_{\boldsymbol{R}}^{\alpha,(n)}$ to the new value $\Omega_{\boldsymbol{R}}^{\alpha,(n+1)}$, the procedure consists of three steps. First, the coherent potential function $\mathcal{P}_{\boldsymbol{R}}^{\alpha,(n)}$ at each site $\boldsymbol{R}$ is set up in terms of $\Omega_{\boldsymbol{R}}^{\alpha,(n)}$ and the potential functions $P_{\boldsymbol{R}}^{\alpha,Q}$ and concentrations $c_{\boldsymbol{R}}^{Q}$ of all components Q according to the relation

$$\left[\mathcal{P}_{\boldsymbol{R}}^{\alpha,(n)} \; - \; \Omega_{\boldsymbol{R}}^{\alpha,(n)} \right]^{-1} \; = \; \sum_{Q} \; c_{\boldsymbol{R}}^{Q} \left[P_{\boldsymbol{R}}^{\alpha,Q} \; - \; \Omega_{\boldsymbol{R}}^{\alpha,(n)} \right]^{-1} \; , \tag{68}$$

or, explicitly,

$$\mathcal{P}_{\boldsymbol{R}}^{\alpha,(n)} \; = \; \left\{ \sum_{Q} \; c_{\boldsymbol{R}}^{Q} \left[P_{\boldsymbol{R}}^{\alpha,Q} \; - \; \Omega_{\boldsymbol{R}}^{\alpha,(n)} \right]^{-1} \right\}^{-1} \; + \; \Omega_{\boldsymbol{R}}^{\alpha,(n)} \; . \tag{69}$$

Second, these coherent potential functions are used to calculate the site-diagonal blocks $\bar{g}_{\boldsymbol{R},\boldsymbol{R}}^{\alpha,(n)}$ of the average auxiliary Green function

$$\bar{g}_{\boldsymbol{R},\boldsymbol{R}}^{\alpha,(n)} \; = \; \left\{ \left[\mathcal{P}^{\alpha,(n)} \; - \; S^{\alpha} \right]^{-1} \right\}_{\boldsymbol{R},\boldsymbol{R}} \; . \tag{70}$$

Third, the new value of the coherent interactor $\Omega_{\boldsymbol{R}}^{\alpha,(n+1)}$ at each site $\boldsymbol{R}$ is obtained from the relation

$$\left[\mathcal{P}_{\boldsymbol{R}}^{\alpha,(n)} \; - \; \Omega_{\boldsymbol{R}}^{\alpha,(n+1)} \right]^{-1} \; = \; \bar{g}_{\boldsymbol{R},\boldsymbol{R}}^{\alpha,(n)} \; , \tag{71}$$

or, explicitly,

$$\Omega_{\boldsymbol{R}}^{\alpha,(n+1)} \; = \; \mathcal{P}_{\boldsymbol{R}}^{\alpha,(n)} \; - \; \left[\bar{g}_{\boldsymbol{R},\boldsymbol{R}}^{\alpha,(n)} \right]^{-1} \; . \tag{72}$$

These three steps have to be repeated in order to obtain converged quantities $\Omega_{\boldsymbol{R}}^{\alpha}$ and $\mathcal{P}_{\boldsymbol{R}}^{\alpha}$ at all sites. Steps (69, 70, 72) preserve the Herglotz property of the matrix quantities $\Omega_{\boldsymbol{R}}^{\alpha}$, $\mathcal{P}_{\boldsymbol{R}}^{\alpha}$, $\bar{g}_{\boldsymbol{R},\boldsymbol{R}}^{\alpha}$. Convergence is achieved typically after 5 to 20 iterations depending on the alloy system and the complex energy variable.

Substantial acceleration of charge selfconsistent calculations for random systems can be achieved by repeated alternation of one CPA iteration and one update of one-electron potentials (see Sect. 5). In such case, the potential functions of all alloy components in (68, 69) are replaced by the n-dependent quantities $P_{\boldsymbol{R}}^{\alpha,Q,(n)}$. The update of the one-electron potentials and the potential functions follows the CPA iteration (69, 70, 72) and is based on charge densities derived from the conditionally averaged local auxiliary Green functions

$$\bar{g}_{\boldsymbol{R},\boldsymbol{R}}^{\alpha,Q} \; = \; \left[P_{\boldsymbol{R}}^{\alpha,Q,(n)} \; - \; \Omega_{\boldsymbol{R}}^{\alpha,(n+1)} \right]^{-1} \; . \tag{73}$$

In this way, the CPA selfconsistency is obtained simultaneously with the LSDA selfconsistency.

4 Surfaces and Interfaces

Applications of the single-site CPA to layered systems on lattices with two-dimensional (2D) translational symmetry require special approaches to calculate the Green function quantities involved. Below we summarize the most essential relations of a technique based on the concept of principal layers and the surface Green functions [26–28].

The approach rests on the use of the tight-binding LMTO representation β which provides the most localized structure constants $S^{\beta}_{\boldsymbol{R}L,\boldsymbol{R}'L'}$ [16,17], and on the representation invariance of the CPA (Sect. 3.3). The finite range of the tight-binding structure constants allows to introduce the principal layers in such a way that (i) each principal layer consists of a finite number of neighboring atomic layers, (ii) the whole lattice can be considered as a stacking of an infinite sequence of the principal layers labeled by an integer index p, see Fig. 3, and (iii) the structure constants $S^{\beta}_{\boldsymbol{R}L,\boldsymbol{R}'L'}$ couple only the neighboring principal layers. The sites $\boldsymbol{R}$ of a given system can be then written in a form $\boldsymbol{R} \equiv (p, \boldsymbol{B}, \boldsymbol{T}_{\parallel})$, where p is the index of the principal layer, $\boldsymbol{B}$ denotes the corresponding basis vector (mostly an atomic layer) in the p-th principal layer, and $\boldsymbol{T}_{\parallel}$ is a 2D translation vector such that $\boldsymbol{R} = \boldsymbol{B} + \boldsymbol{T}_{\parallel}$. We assume for simplicity that each principal layer contains the same number n_{B} of the basis vectors $\boldsymbol{B}$.

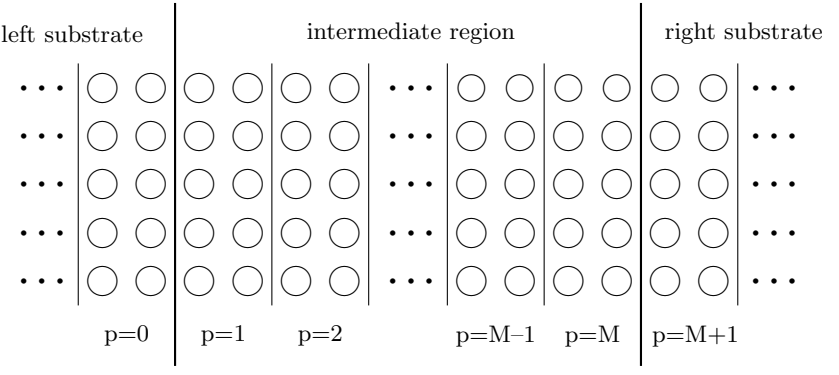

Fig. 3. Principal layers for a single interface of two semi-infinite systems

As a consequence of the 2D translational symmetry of the lattice, a 2D lattice Fourier transformation of the structure constant matrix leads to a $\boldsymbol{k}_{\parallel}$-dependent matrix

$$S^{\beta}_{p\boldsymbol{B}L,p'\boldsymbol{B}'L'}(\boldsymbol{k}_{\parallel}) \;=\; \sum_{\boldsymbol{T}_{\parallel}} S^{\beta}_{p\boldsymbol{B}L,p'(\boldsymbol{B}'+\boldsymbol{T}_{\parallel})L'} \;\exp(\mathrm{i}\,\boldsymbol{k}_{\parallel}\cdot\boldsymbol{T}_{\parallel})\;, \tag{74}$$

where $\boldsymbol{k}_{\parallel}$ denotes a vector in the 2D BZ. It should be noted that the tight-binding structure constants (74) vanish for $|p - p'| > 1$, i.e., they form a block

tridiagonal matrix with respect to the principal-layer index. In the following, we will often omit the composed matrix index $\boldsymbol{B}L$ so that matrix quantities with elements $X_{p\boldsymbol{B}L,p'\boldsymbol{B}'L'}$ and $W_{p,\boldsymbol{B}L,\boldsymbol{B}'L'}$ will be respectively abbreviated as $X_{p,p'}$ and W_p. The dimension of the latter matrices is equal to $n_{\mathrm{B}}(\ell_{\max}+1)^2$, where $\ell_{\max}$ denotes the angular-momentum cutoff.

Let us consider the case of a single interface of two semi-infinite systems. Examples of this situation are: a surface of a bulk alloy (solid-vacuum interface), an epitaxial interface of two alloys (metals), a special grain boundary in a bulk metal, etc. The treatment of all these cases can be greatly simplified due to the fact that all inhomogeneities are confined to an intermediate region of a finite thickness (principal layers $1 \le p \le M$) placed between two semi-infinite substrates, see Fig. 3. The electronic properties (e.g., the coherent potential functions) of both unperturbed substrates are supposed to be known and the main interest then concentrates on the intermediate region. Let us assume that the configuration-independent properties of the layered alloy system exhibit the 2D translational symmetry of the underlying lattice. As a consequence, the coherent potential functions for all lattice sites reduce to $p\boldsymbol{B}$-resolved quantities $\mathcal{P}^{\beta}_{p\boldsymbol{B},LL'}(z)$ which form matrices $\mathcal{P}^{\beta}_{p}(z)$ with elements $\mathcal{P}^{\beta}_{p,\boldsymbol{B}L,\boldsymbol{B}'L'}(z) = \mathcal{P}^{\beta}_{p\boldsymbol{B},LL'}(z)\,\delta_{\boldsymbol{B}\boldsymbol{B}'}$. The average auxiliary Green function (24) can be then calculated using the corresponding lattice Fourier transform $\bar{g}^{\beta}_{p\boldsymbol{B}L,p'\boldsymbol{B}'L'}(\boldsymbol{k}_{\parallel},z)$.

The layer-diagonal ($p = p'$) blocks of the latter can be expressed as

$$\begin{aligned}\bar{g}^{\beta}_{p,p}(\boldsymbol{k}_{\parallel},z) \;=\; \Big[\; & \mathcal{P}^{\beta}_{p}(z) \;-\; S^{\beta}_{p,p}(\boldsymbol{k}_{\parallel}) \\ & -\; \Gamma^{\beta,<}_{p}(\boldsymbol{k}_{\parallel},z) \;-\; \Gamma^{\beta,>}_{p}(\boldsymbol{k}_{\parallel},z) \Big]^{-1} ,\end{aligned} \tag{75}$$

where the the first two terms in the bracket correspond to the isolated p-th layer while the so-called embedding potentials $\Gamma^{\beta,<}_{p}(\boldsymbol{k}_{\parallel},z)$ and $\Gamma^{\beta,>}_{p}(\boldsymbol{k}_{\parallel},z)$ reflect the influence of the two semi-infinite parts adjacent to the p-th principal layer – the superscript $<$ ($>$) refers to the part consisting of all principal layers $p' < p$ ($p' > p$). The embedding potentials for layers inside the intermediate region ($1 \le p \le M$) can be calculated from recursion relations

$$\begin{aligned}\Gamma^{\beta,<}_{p}(\boldsymbol{k}_{\parallel},z) \;=\; & S^{\beta}_{p,p-1}(\boldsymbol{k}_{\parallel}) \Big[\; \mathcal{P}^{\beta}_{p-1}(z) \;-\; S^{\beta}_{p-1,p-1}(\boldsymbol{k}_{\parallel}) \\ & -\; \Gamma^{\beta,<}_{p-1}(\boldsymbol{k}_{\parallel},z) \Big]^{-1} S^{\beta}_{p-1,p}(\boldsymbol{k}_{\parallel}) , \\ \Gamma^{\beta,>}_{p}(\boldsymbol{k}_{\parallel},z) \;=\; & S^{\beta}_{p,p+1}(\boldsymbol{k}_{\parallel}) \Big[\; \mathcal{P}^{\beta}_{p+1}(z) \;-\; S^{\beta}_{p+1,p+1}(\boldsymbol{k}_{\parallel}) \\ & -\; \Gamma^{\beta,>}_{p+1}(\boldsymbol{k}_{\parallel},z) \Big]^{-1} S^{\beta}_{p+1,p}(\boldsymbol{k}_{\parallel}) ,\end{aligned} \tag{76}$$

and from the starting values

$$\begin{aligned}\Gamma^{\beta,<}_{1}(\boldsymbol{k}_{\parallel},z) \;&=\; S^{\beta}_{1,0}(\boldsymbol{k}_{\parallel})\; \mathcal{G}^{\beta}_{\mathrm{left}}(\boldsymbol{k}_{\parallel},z)\; S^{\beta}_{0,1}(\boldsymbol{k}_{\parallel}) , \\ \Gamma^{\beta,>}_{M}(\boldsymbol{k}_{\parallel},z) \;&=\; S^{\beta}_{M,M+1}(\boldsymbol{k}_{\parallel})\; \mathcal{G}^{\beta}_{\mathrm{right}}(\boldsymbol{k}_{\parallel},z)\; S^{\beta}_{M+1,M}(\boldsymbol{k}_{\parallel}) .\end{aligned} \tag{77}$$

The matrix quantities $\mathcal{G}^{\beta}_{\rm left}(\boldsymbol{k}_{\parallel}, z)$ and $\mathcal{G}^{\beta}_{\rm right}(\boldsymbol{k}_{\parallel}, z)$ in (77) are the surface Green functions of the two semi-infinite substrates sandwiching the intermediate region. The calculation of the layer-diagonal blocks of the Green function according to (75, 76) is obviously an order-M procedure.

The surface Green function (SGF) is defined as a projection of the full Green function of a semi-infinite layered system onto its outer principal layer. For a semi-infinite system consisting of identical principal layers, one can apply the concept of removal invariance [2] to derive a closed condition for the SGF which reflects the true semi-infinite geometry of the system. In the case of the left substrate in Fig. 3, this condition is

$$\mathcal{G}^{\beta}_{\rm left}(\boldsymbol{k}_{\parallel}, z) \;=\; \Big[\, \mathcal{P}^{\beta}_{0}(z) \;-\; S^{\beta}_{0,0}(\boldsymbol{k}_{\parallel}) \;- S^{\beta}_{0,-1}(\boldsymbol{k}_{\parallel})\; \mathcal{G}^{\beta}_{\rm left}(\boldsymbol{k}_{\parallel}, z)\; S^{\beta}_{-1,0}(\boldsymbol{k}_{\parallel}) \,\Big]^{-1} , \tag{78}$$

whereas an analogous condition for the right substrate is omitted here for brevity. Both conditions are of the same form, namely

$$\mathcal{G} \;=\; (D \;-\; A\,\mathcal{G}\,B)^{-1} , \tag{79}$$

where $\mathcal{G}$ is the SGF and where the $\boldsymbol{k}_{\parallel}$- and z-arguments were suppressed. The most direct method to solve (79) is based on simple iterations [28]

$$\mathcal{G}^{(n+1)} \;=\; (D \;-\; A\,\mathcal{G}^{(n)}\,B)^{-1} \tag{80}$$

starting from an input value $\mathcal{G}^{(0)}$ which can be set either to zero or, e.g., to the converged SGF for a neighboring energy argument. The latter choice of $\mathcal{G}^{(0)}$ substantially reduces the number of necessary iteration steps, especially for complex energies close to the real axis. The iterative procedure (80) is easy to implement, leads always to the correct solution of (79) satisfying the Herglotz property, and has a direct physical meaning: $\mathcal{G}^{(n)}$ with the initial value $\mathcal{G}^{(0)} = 0$ corresponds to the SGF of a stacking of n identical principal layers. The number of steps to get a converged SGF depends on the imaginary part of the complex energy z, but in most applications several tens of iterations are sufficient. In the cases where an enhanced accuracy of the SGF and/or very small $\mathrm{Im}\, z$ (less than 10 mRy) are needed, the SGF can be more efficiently obtained by means of the renormalization-decimation technique [15,18,29]. The high efficiency of the latter method is due to an exponential increase of the thickness of an effective layer with the number of iterations, in contrast to the linear increase inherent to the simple procedure (80).

For evaluation of local physical observables as well as for the solution of the CPA condition, the site-diagonal blocks of the average auxiliary Green function are of central importance (see Sect. 3). They can be obtained by a 2D BZ-integration of (75) as

$$\bar{g}^{\beta}_{p\boldsymbol{B}L,p\boldsymbol{B}L'}(z) \;=\; \frac{1}{N_{\parallel}} \sum_{\boldsymbol{k}_{\parallel}} \bar{g}^{\beta}_{p\boldsymbol{B}L,p\boldsymbol{B}L'}(\boldsymbol{k}_{\parallel}, z) \;, \tag{81}$$

where $N_\parallel$ is the number of $\boldsymbol{k}_\parallel$-points sampling the 2D BZ. The layer-diagonal $\boldsymbol{k}_\parallel$-dependent average auxiliary Green functions (75) enter also the corresponding Bloch spectral functions ($\boldsymbol{k}_\parallel$-resolved densities of states). They are defined in analogy to (56) as

$$\mathcal{A}_{p\boldsymbol{B}L}(\boldsymbol{k}_\parallel, E) \;=\; -\,\frac{1}{\pi}\,\mathrm{Im}\;\bar{G}_{p\boldsymbol{B}L,p\boldsymbol{B}L}(\boldsymbol{k}_\parallel, E+\mathrm{i}0)\;, \tag{82}$$

where the lattice Fourier transform of the average physical Green function is given by (cf. (57))

$$\begin{aligned}\bar{G}_{p\boldsymbol{B}L,p\boldsymbol{B}L}(\boldsymbol{k}_\parallel, z) \;=\; \sum_{L'L''} \tilde{\mathcal{M}}^{\beta}_{p\boldsymbol{B},LL'}(z)\;\bar{g}^{\beta}_{p\boldsymbol{B}L',p\boldsymbol{B}L''}(\boldsymbol{k}_\parallel, z)\;\mathcal{M}^{\beta}_{p\boldsymbol{B},L''L}(z) \\ +\;\mathcal{L}^{\beta}_{p\boldsymbol{B},LL}(z)\;.\end{aligned} \tag{83}$$

It should be noted that the Bloch spectral functions (82) represent a suitable tool to study surface/interface states in disordered as well as ordered layered systems.

Figure 4 shows the local densities of states at the (001) surface of a random non-magnetic bcc $Fe_{0.15}V_{0.85}$ alloy. One can clearly see a rapid convergence of the layer-resolved densities to their bulk counterparts, which justifies numerically the concept of the intermediate region of a finite thickness. The bands in the top surface layer are narrower than the bulk ones and the pronounced minima in the middle of the bcc bulk bands are absent in the top surface layer. These effects can be ascribed to the reduced coordination of the surface atoms. As a consequence, both components exhibit a strong enhancement of the surface densities of states at the Fermi energy (see Fig. 4) which in turn can induce a surface magnetic instability of the non-magnetic bulk alloy.

5 Charge Selfconsistency for Random Alloys

The LSDA selfconsistency for substitutionally disordered systems within the CPA and the ASA is based on the average component-resolved charge densities (42). In the following formulas, we use atomic Rydberg units ($e^2 = 2$) and assume a spin-polarized non-relativistic system with a collinear spin structure. The spin-dependent charge densities inside the individual atomic spheres will be denoted $\varrho^{Q}_{\boldsymbol{R}\sigma}(\boldsymbol{r})$ where $\sigma = \uparrow, \downarrow$ is the spin index. Related quantities are the spherically averaged spin-dependent densities

$$\tilde{\varrho}^{Q}_{\boldsymbol{R}\sigma}(r) \;=\; \frac{1}{4\pi}\int \varrho^{Q}_{\boldsymbol{R}\sigma}(\boldsymbol{r})\;d^2\hat{\boldsymbol{r}}\;, \tag{84}$$

and the total electronic charge densities

$$\varrho^{Q}_{\boldsymbol{R}}(\boldsymbol{r}) \;=\; \varrho^{Q}_{\boldsymbol{R}\uparrow}(\boldsymbol{r}) + \varrho^{Q}_{\boldsymbol{R}\downarrow}(\boldsymbol{r})\;, \qquad \tilde{\varrho}^{Q}_{\boldsymbol{R}}(r) \;=\; \tilde{\varrho}^{Q}_{\boldsymbol{R}\uparrow}(r) + \tilde{\varrho}^{Q}_{\boldsymbol{R}\downarrow}(r)\;. \tag{85}$$

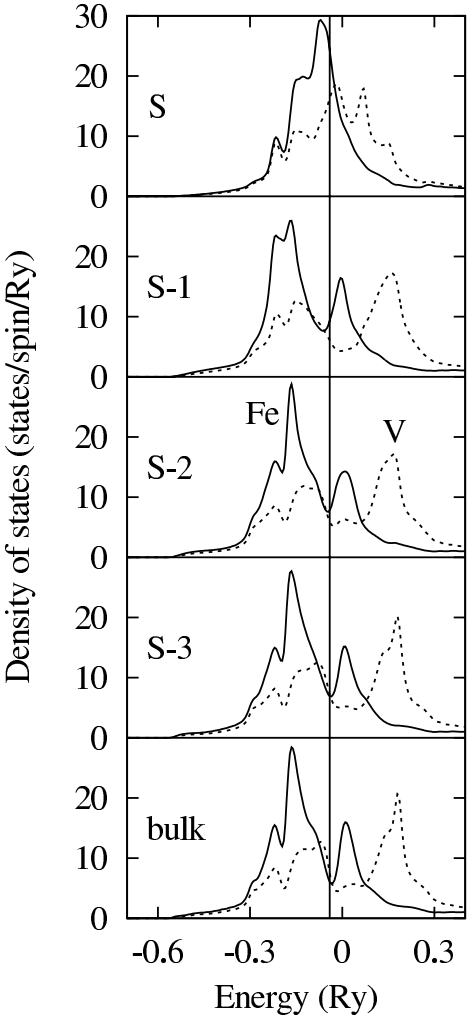

Fig. 4. Layer-resolved local densities of states for Fe (*full lines*) and V (*dotted lines*) atoms at the (001) surface of the random bcc $Fe_{0.15}V_{0.85}$ alloy. The top four layers and the bulk layer are denoted by S, S-1, S-2, S-3, and bulk, respectively. The vertical line denotes the position of the Fermi energy

The selfconsistent one-electron component-dependent ASA potentials are then given by

$$V^Q_{\boldsymbol{R}\sigma}(r) \;=\; -\,2\,Z^Q_{\boldsymbol{R}}\,r^{-1} \;+\; \int_{(\boldsymbol{R})} 2\,\tilde{\varrho}^Q_{\boldsymbol{R}}(r')\;|\boldsymbol{r}-\boldsymbol{r}'|^{-1}\;d^3\boldsymbol{r}' \\ +\; V_{\mathrm{xc},\sigma}\big(\tilde{\varrho}^Q_{\boldsymbol{R}\uparrow}(r),\tilde{\varrho}^Q_{\boldsymbol{R}\downarrow}(r)\big) \;+\; V_{\mathrm{Mad},\boldsymbol{R}s}\;, \tag{86}$$

where the integration is carried out over the $\boldsymbol{R}$-th atomic sphere. The first term in (86) is the Coulomb potential due to the point-like nuclear charge $Z^Q_{\boldsymbol{R}}$, the second term is the Hartree potential due to the spherically symmetric charge density $\tilde{\varrho}^Q_{\boldsymbol{R}}(r)$, the third term represents the exchange-correlation contribution, and the last term is the Madelung contribution. The exchange-correlation term

is evaluated according to a standard relation

$$V_{\mathrm{xc},\sigma}(\varrho_\uparrow,\varrho_\downarrow) \;=\; \frac{\partial}{\partial\varrho_\sigma}\left[\,(\varrho_\uparrow+\varrho_\downarrow)\,\varepsilon_{\mathrm{xc}}(\varrho_\uparrow,\varrho_\downarrow)\,\right]\;, \tag{87}$$

where $\varepsilon_{\mathrm{xc}}(\varrho_\uparrow,\varrho_\downarrow)$ is the exchange-correlation energy per particle of a spin-polarized homogeneous electron gas. The Madelung contribution $V_{\mathrm{Mad},\boldsymbol{R}s}$ in (86) is a special case (for $L=(\ell,m)=(0,0)$) of the multipole Madelung terms defined by

$$V_{\mathrm{Mad},\boldsymbol{R}L} \;=\; {\sum_{\boldsymbol{R}'L'}}' \; M_{\boldsymbol{R}L,\boldsymbol{R}'L'}\;\bar{q}_{\boldsymbol{R}'L'}\;, \tag{88}$$

where the primed sum indicates exclusion of the term $\boldsymbol{R}'=\boldsymbol{R}$. The constants $M_{\boldsymbol{R}L,\boldsymbol{R}'L'}$ in (88) describe the electrostatic interactions between two multipoles located at the sites $\boldsymbol{R},\boldsymbol{R}'$ and the quantities $\bar{q}_{\boldsymbol{R}L}$ are average multipole moments due to the total (electronic and nuclear) charge densities inside the atomic spheres,

$$\begin{aligned}
\bar{q}_{\boldsymbol{R}L} \;&=\; \sum_Q \; c^Q_{\boldsymbol{R}}\; q^Q_{\boldsymbol{R}L}\;,\\
q^Q_{\boldsymbol{R}L} \;&=\; \sqrt{\frac{4\pi}{2\ell+1}}\;\int_{(\boldsymbol{R})}\; r^\ell\; Y_L(\hat{\boldsymbol{r}})\;\varrho^Q_{\boldsymbol{R}}(\boldsymbol{r})\;d^3\boldsymbol{r}\;-\;Z^Q_{\boldsymbol{R}}\,\delta_{\ell,0}\;.
\end{aligned} \tag{89}$$

Let us note that $\bar{q}_{\boldsymbol{R}s}$ and $q^Q_{\boldsymbol{R}s}$ ($\ell=0$ in (89)) refer to the net charges inside the $\boldsymbol{R}$-th sphere. The summations in (88) for infinite lattices with two- or three-dimensional translational symmetry can be performed using the corresponding Ewald techniques [15,18,30]. For bulk systems the Madelung contribution (88) is often calculated only from the net charges $\bar{q}_{\boldsymbol{R}s}$, whereas for surfaces an inclusion of the dipole moments is inevitable, e.g., for a good description of the surface dipole barrier and the work function [30].

For calculations of charge densities, the energy dependence of the regular radial amplitude in (3) is replaced by a truncated Taylor expansion at an energy $E^Q_{\nu,\boldsymbol{R}\ell\sigma}$ in the center of the occupied part of the valence band

$$\begin{aligned}
\varphi^Q_{\boldsymbol{R}\ell\sigma}(r,E) \;&=\; \phi^Q_{\boldsymbol{R}\ell\sigma}(r)\;+\;\dot{\phi}^Q_{\boldsymbol{R}\ell\sigma}(r)\,\left(E-E^Q_{\nu,\boldsymbol{R}\ell\sigma}\right)\\
&\quad+\;\frac{1}{2}\,\ddot{\phi}^Q_{\boldsymbol{R}\ell\sigma}(r)\,\left(E-E^Q_{\nu,\boldsymbol{R}\ell\sigma}\right)^2\;,
\end{aligned} \tag{90}$$

which results in a simple expression for the spherically averaged charge density (84)

$$\begin{aligned}
\tilde{\varrho}^Q_{\boldsymbol{R}\sigma}(r) \;&=\; \frac{1}{4\pi}\sum_\ell\;\Big\{\; m^{Q,0}_{\boldsymbol{R}\ell\sigma}\;\left(\phi^Q_{\boldsymbol{R}\ell\sigma}(r)\right)^2\;+\;2\,m^{Q,1}_{\boldsymbol{R}\ell\sigma}\;\phi^Q_{\boldsymbol{R}\ell\sigma}(r)\;\dot{\phi}^Q_{\boldsymbol{R}\ell\sigma}(r)\\
&\qquad+\;m^{Q,2}_{\boldsymbol{R}\ell\sigma}\;\left[\left(\dot{\phi}^Q_{\boldsymbol{R}\ell\sigma}(r)\right)^2\;+\;\phi^Q_{\boldsymbol{R}\ell\sigma}(r)\;\ddot{\phi}^Q_{\boldsymbol{R}\ell\sigma}(r)\right]\;\Big\}\\
&\quad+\;\varrho^{Q,\mathrm{core}}_{\boldsymbol{R}\sigma}(r)\;.
\end{aligned} \tag{91}$$

In (91) the last term denotes the core contribution while the quantities $m^{Q,k}_{\boldsymbol{R}\ell\sigma}$ $(k = 0, 1, 2)$ represent the lowest energy moments of the $Q\boldsymbol{R}\ell\sigma$-projected valence densities of states (41)

$$m^{Q,k}_{\boldsymbol{R}\ell\sigma} \;=\; \int_{E_B}^{E_F} \left(E - E^Q_{\nu,\boldsymbol{R}\ell\sigma}\right)^k \sum_{m=-\ell}^{\ell} n^Q_{\boldsymbol{R}L\sigma}(E)\; dE \;, \tag{92}$$

where E_B denotes the bottom of the valence band. Similarly, the multipole moments $q^Q_{\boldsymbol{R}L}$ (89) reduce to several radial and energy integrations [15,30]. The latter are of the type $(k, k' = 0, 1, 2)$

$$m^{Q,kk'}_{\boldsymbol{R},LL',\sigma} \;=\; \int_{E_B}^{E_F} \left(E - E^Q_{\nu,\boldsymbol{R}\ell\sigma}\right)^k n^Q_{\boldsymbol{R},LL',\sigma}(E) \left(E - E^Q_{\nu,\boldsymbol{R}\ell'\sigma}\right)^{k'} dE \tag{93}$$

representing thus the lowest energy moments of the local density of states matrix $n^Q_{\boldsymbol{R},LL',\sigma}(E)$ (40).

As follows from (40), the energy integrals (92, 93) over the occupied part of the valence spectrum can be generally formulated as

$$-\,\frac{1}{\pi}\int_{E_B}^{E_F} \mathrm{Im}\; F(E + \mathrm{i}0)\; dE \;=\; \frac{1}{2\pi\mathrm{i}}\int_C F(z)\; dz \;. \tag{94}$$

The function $F(z)$ is an analytic function of the complex energy variable z (except at poles and/or branch cuts lying on the real energy axis) which satisfies $F(z^*) = F^*(z)$. The r.h.s. integral in (94) is taken along a closed contour C intersecting the real energy axis at the Fermi level and enclosing the occupied valence band. Standard quadrature techniques lead to an approximation

$$\frac{1}{2\pi\mathrm{i}}\int_C F(z)\; dz \;\approx\; \mathrm{Re}\left[\sum_{n=1}^{N} w_n\; F(z_n)\right] \;, \tag{95}$$

which replaces the original integral along the real axis by a finite sum with N complex weights w_n and nodes $z_n \in C$. All nodes z_n can be chosen in the upper (or the lower) complex halfplane. They are usually taken along a semicircle contour with a denser mesh near the Fermi energy. Experience shows that a relatively modest number of nodes ($N \sim 10$ to 20) is sufficient to achieve desired accuracy in most charge selfconsistent calculations. Minor complications arise in selfconsistent bulk calculations in which the Fermi energy E_F is unknown and changes in each iteration (contrary to the case of surfaces where the value of E_F is fixed from a previous calculation of the bulk substrate). Fortunately, it is not necessary to locate the bulk Fermi level exactly in each iteration but merely to update its value so that the convergence of E_F proceeds simultaneously with that of the one-electron potentials.

Iterative procedures leading to selfconsistent one-electron potentials (or charge densities) have been recently systematically accelerated by means of quasi-Newton methods (like the Anderson and the second Broyden mixing scheme) [31]. These

techniques are efficient also for random alloy systems where the LSDA-CPA selfconsistency can be achieved by alternating updates of the one-electron potentials and the coherent interactors (Sect. 3.4). According to our experience, the full convergence in all-electron calculations can be obtained in 30 to 80 iterations for most systems.

The total energy for non-random systems within the ASA [17,20,30] can be directly generalized to the case with substitutional randomness. The final formula is given by a concentration-weighted sum of $\boldsymbol{R}Q$-dependent terms

$$\mathcal{E} \;=\; \sum_{\boldsymbol{R}Q} c^Q_{\boldsymbol{R}}\; \mathcal{E}^Q_{\boldsymbol{R}} \;, \tag{96}$$

where the individual contributions $\mathcal{E}^Q_{\boldsymbol{R}}$ are explicitly given by

$$\begin{aligned}
\mathcal{E}^Q_{\boldsymbol{R}} \;=\; & \sum_{\sigma j} \epsilon^{Q,\mathrm{core}}_{\boldsymbol{R}\sigma j} \;+\; \sum_{L\sigma} \int_{E_B}^{E_F} E\; n^Q_{\boldsymbol{R}L\sigma}(E)\; dE \\
& - \sum_{\sigma} \int_{(\boldsymbol{R})} \tilde{\varrho}^Q_{\boldsymbol{R}\sigma}(r)\; V^Q_{\boldsymbol{R}\sigma}(r)\; d^3\boldsymbol{r} \\
& + \int_{(\boldsymbol{R})} \tilde{\varrho}^Q_{\boldsymbol{R}}(r)\; \Big[\, \varepsilon_{\mathrm{xc}}\big(\tilde{\varrho}^Q_{\boldsymbol{R}\uparrow}(r), \tilde{\varrho}^Q_{\boldsymbol{R}\downarrow}(r)\big) \;-\; 2\, Z^Q_{\boldsymbol{R}}\, r^{-1} \,\Big]\; d^3\boldsymbol{r} \\
& + \int_{(\boldsymbol{R})} \int_{(\boldsymbol{R})} \tilde{\varrho}^Q_{\boldsymbol{R}}(r)\; \tilde{\varrho}^Q_{\boldsymbol{R}}(r')\; |\boldsymbol{r} - \boldsymbol{r}'|^{-1}\; d^3\boldsymbol{r}\; d^3\boldsymbol{r}' \\
& + \frac{1}{2} \sum_{L} q^Q_{\boldsymbol{R}L}\; V_{\mathrm{Mad},\boldsymbol{R}L} \;.
\end{aligned} \tag{97}$$

The first term in (97) is the sum of core eigenvalues $\epsilon^{Q,\mathrm{core}}_{\boldsymbol{R}\sigma j}$ labeled by j, while the second term represents an energy contribution due to the valence densities of states $n^Q_{\boldsymbol{R}L\sigma}(E)$ (41). It can be trivially expressed in terms of the moments $m^{Q,k}_{\boldsymbol{R}\ell\sigma}$ (92).

Let us note that the above presented formulas for the one-electron potentials (86) and for the total-energy contributions (97) were derived under a complete neglect of any correlations (i) between the occupation of a particular site $\boldsymbol{R}$ and the charge densities inside the other atomic spheres, and (ii) between the charge densities inside different atomic spheres. These neglected correlations result then in the component-independent Madelung terms $V_{\mathrm{Mad},\boldsymbol{R}L}$ (88) due to the average multipole moments $\bar{q}_{\boldsymbol{R}'L'}$ (89). This simple treatment is fully compatible with the mean-field nature of the single-site CPA.

However, it has been found in a number of applications of the CPA that the neglected charge correlations lead to substantial errors in the calculated total energies. Several schemes were suggested to remove this drawback. Let us consider for simplicity only the case of random binary bcc or fcc alloys. The condition of the overall charge neutrality together with the neglect of higher multipole moments leads to a vanishing mean-field Madelung contribution $V_{\mathrm{Mad},s}$

to the one-electron potential (the site index $\boldsymbol{R}$ is omitted). The screened CPA [32] and the screened impurity model [33] lead to a component-dependent Madelung term

$$V^Q_{\mathrm{Mad},s} \;=\; -\,2\,q^Q_s\,d^{-1}_{\mathrm{nn}}\;, \tag{98}$$

where d_{nn} denotes the distance between the nearest neighboring sites of the lattice. This shift of the one-electron potentials follows from an assumption of a perfect screening of the net charge q^Q_s by compensating charges located on the nearest neighbors. The correction to the total alloy energy per lattice site is then given by

$$\Delta\mathcal{E}_1 \;=\; \beta\,\sum_Q c^Q\,q^Q_s\,V^Q_{\mathrm{Mad},s}\;, \tag{99}$$

where the prefactor β equals $1/2$ for the screened CPA [32,34] whereas for the screened impurity model the whole interval $1/2 \le \beta \le 1$ was considered [33,35,36]. Another approach employs an idea of neutral atomic spheres [37,38] where the sphere radii s^Q are changed (keeping the average atomic volume fixed) to achieve vanishing net charges ($q^Q_s = 0$) for both alloy components. All of these schemes improve considerably the calculated total energies for many alloy systems but a detailed assessment of their validity especially for alloy surfaces remains yet to be done.

6 Extensions and Applications of the LMTO-CPA

The non-relativistic TB-LMTO-CPA theory of substitutionally disordered alloys can be generalized to include properly all relativistic effects based on the Dirac equation. The relativistic theory in the non-magnetic case represents a straightforward modification of the non-relativistic counterpart [15,39] whereas for spin-polarized systems certain theoretical as well as technical problems appear [15,40]. Nevertheless, many of the theoretical concepts introduced above remain valid.

The energetics of metallic alloys and their surfaces with applications to ordering and segregation phenomena is usually studied in terms of effective interatomic interactions. They can be determined from ab initio electronic structure calculations using either the generalized perturbation method [23] or the Connolly-Williams inversion scheme [41]. In the context of the LMTO-CPA theory, the generalized perturbation method was described in [15,42] and reviewed in [43], while a modification of the Connolly-Williams approach was developed in [44].

Recent applications of the selfconsistent LMTO-CPA method cover a large area of the modern theory of alloys. The ground-state properties of non-magnetic bulk random alloys were investigated, e.g., in [33,35,38], while the Fermi surfaces and the electronic topological transitions were studied in [45]. Existing applications to magnetic bulk alloys include studies of the local magnetic moments [40,46], various aspects of the Invar alloys [47,48], the structural stability [49,50], the ordering tendencies [49,51,52], and the Curie temperatures [43].

The electronic structure of surfaces of random alloys was investigated, e.g., in [39,53–55], studies of the surface segregation were published in [42–44,54,56,57], and calculations of the surface magnetic properties of random alloys were presented in [58,59].

Two-dimensional random alloys which can be formed at an epitaxial interface of two different metals represent another field of applicability of the LMTO-CPA method. The electronic structure of non-magnetic random overlayers on metallic substrates was calculated, e.g., in [55,60,61] while random magnetic overlayers on non-magnetic substrates were studied in [46,62,63]. The adlayer core-level shifts of random overlayers were calculated in [64], the ordering tendencies in surface non-magnetic alloys were analysed in [65], the interplay of magnetism and ordering was considered in [51], and the stability of metallic interfaces was investigated in [66].

The interlayer exchange coupling, encountered in epitaxial magnetic multilayers, is another quantity which can be influenced by substitutional disorder both in the magnetic layers and in the non-magnetic spacer. Applications of the LMTO-CPA to this problem can be found in the review [67] and references therein.

The formalism presented in this paper as well as the applications listed above are heavily based on the ASA. A development of a full-potential version of the LMTO-CPA is difficult due to the dependence of each LMTO on the occupation of all lattice sites. This complicated configuration dependence of the LMTO's can be removed in the so-called pure-L approximation for the TB-LMTO's [68] and the corresponding single-site CPA theory can be then derived. This was done in [69,70] together with applications to random fcc Li-Al and Ni-Pt bulk alloys.

Acknowledgements This work is a part of activities of the Center for Computational Materials Science sponsored by the Academy of Sciences of the Czech Republic. This research was supported by the Grant Agency of the Czech Republic (Project 202/97/0598), the Grant Agency of the Academy of Sciences of the Czech Republic (Project A1010829), and the Czech Ministry of Education, Youth, and Sports (in the framework of the COST Action P3 'Simulation of physical phenomena in technological applications').

References

1. P. Weinberger, Electron Scattering Theory for Ordered and Disordered Matter (Clarendon Press, Oxford, 1990).
2. A. Gonis, Green Functions for Ordered and Disordered Systems (North-Holland, Amsterdam, 1992).
3. O.K. Andersen, Phys. Rev. B **12**, 3060 (1975).
4. H.L. Skriver, The LMTO Method (Springer, Berlin, 1984).
5. D.J. Singh, Planewaves, Pseudopotentials and the LAPW Method (Kluwer Academic Publishers, Boston, 1994).

6. H. Eschrig, Optimized LCAO Method and the Electronic Structure of Extended Systems (Springer, Berlin, 1989).
7. P. Soven, Phys. Rev. **156**, 809 (1967).
8. B. Velický, S. Kirkpatrick, and H. Ehrenreich, Phys. Rev. **175**, 747 (1968).
9. J.A. Blackman, D.M. Esterling, and N.F. Berk, Phys. Rev. B **4**, 2412 (1971).
10. J.S. Faulkner and G.M. Stocks, Phys. Rev. B **21**, 3222 (1980).
11. J.S. Faulkner, Prog. Mater. Sci. **27**, 1 (1982).
12. R. Richter, H. Eschrig, and B. Velický, J. Phys. F: Met. Phys. **17**, 351 (1987).
13. K. Koepernik, B. Velický, R. Hayn, and H. Eschrig, Phys. Rev. B **55**, 5717 (1997).
14. J. Kudrnovský and V. Drchal, Phys. Rev. B **41**, 7515 (1990).
15. I. Turek, V. Drchal, J. Kudrnovský, M. Šob, and P. Weinberger, Electronic Structure of Disordered Alloys, Surfaces and Interfaces (Kluwer Academic Publishers, Boston, 1997).
16. O.K. Andersen and O. Jepsen, Phys. Rev. Lett. **53**, 2571 (1984).
17. O.K. Andersen, O. Jepsen, and M. Šob, in: Electronic Band Structure and Its Applications, edited by M. Yussouff (Springer, Berlin, 1987) p. 1.
18. V. Drchal, J. Kudrnovský, and I. Turek, Comput. Phys. Commun. **97**, 111 (1996).
19. C. Koenig and E. Daniel, J. Physique Lettres **42**, L 193 (1981).
20. O. Gunnarsson, O. Jepsen, and O.K. Andersen, Phys. Rev. B **27**, 7144 (1983).
21. V. Drchal, J. Kudrnovský, L. Udvardi, P. Weinberger, and A. Pasturel, Phys. Rev. B **45**, 14328 (1992).
22. F. Ducastelle, J. Phys. C: Solid State Phys. **8**, 3297 (1975).
23. F. Ducastelle and F. Gautier, J. Phys. F: Met. Phys. **6**, 2039 (1976).
24. F. Ducastelle, Order and Phase Stability (North-Holland, Amsterdam, 1991).
25. K.C. Hass, B. Velický, and H. Ehrenreich, Phys. Rev. B **29**, 3697 (1984).
26. B. Velický and J. Kudrnovský, Surf. Sci. **64**, 411 (1977).
27. J. Kudrnovský, P. Weinberger, and V. Drchal, Phys. Rev. B **44**, 6410 (1991).
28. B. Wenzien, J. Kudrnovský, V. Drchal, and M. Šob, J. Phys.: Condens. Matter **1**, 9893 (1989).
29. M.P. López Sancho, J.M. López Sancho, and J. Rubio, J. Phys. F: Metal Phys. **15**, 851 (1985).
30. H.L. Skriver and N.M. Rosengaard, Phys. Rev. B **43**, 9538 (1991).
31. V. Eyert, J. Comput. Phys. **124**, 271 (1996).
32. D.D. Johnson and F.J. Pinski, Phys. Rev. B **48**, 11553 (1993).
33. P.A. Korzhavyi, A.V. Ruban, I.A. Abrikosov, and H.L. Skriver, Phys. Rev. B **51**, 5773 (1995).
34. F.J. Pinski, J.B. Staunton, and D.D. Johnson, Phys. Rev. B **57**, 15177 (1998).
35. A.V. Ruban, I.A. Abrikosov, and H.L. Skriver, Phys. Rev. B **51**, 12958 (1995).
36. I.A. Abrikosov and B. Johansson, Phys. Rev. B **57**, 14164 (1998).
37. A. Gonis, P.E.A. Turchi, J. Kudrnovský, V. Drchal, and I. Turek, J. Phys.: Condens. Matter **8**, 7869 (1996).
38. A. Gonis, P.E.A. Turchi, J. Kudrnovský, V. Drchal, and I. Turek, J. Phys.: Condens. Matter **8**, 7883 (1996).
39. V. Drchal, J. Kudrnovský, and P. Weinberger, Phys. Rev. B **50**, 7903 (1994).
40. A.B. Shick, V. Drchal, J. Kudrnovský, and P. Weinberger, Phys. Rev. B **54**, 1610 (1996).
41. J.W.D. Connolly and A.R. Williams, Phys. Rev. B **27**, 5169 (1983).
42. V. Drchal, J. Kudrnovský, A. Pasturel, I. Turek, and P. Weinberger, Phys. Rev. B **54**, 8202 (1996).

43. V. Drchal, J. Kudrnovský, A. Pasturel, I. Turek, P. Weinberger, A. Gonis, and P.E.A. Turchi, in: Tight-Binding Approach to Computational Materials Science, edited by P.E.A. Turchi, A. Gonis, and L. Colombo, MRS Symp. Proc. Vol. **491** (Materials Research Society, Warrendale, 1998), p. 65.
44. A.V. Ruban, I.A. Abrikosov, D. Ya. Kats, D. Gorelikov, K.W. Jacobsen, and H.L. Skriver, Phys. Rev. B **49**, 11383 (1994).
45. N.V. Skorodumova, S.I. Simak, I.A. Abrikosov, B. Johansson, and Yu. Kh. Vekilov, Phys. Rev. B **57**, 14673 (1998).
46. I. Turek, J. Kudrnovský, V. Drchal, and P. Weinberger, Phys. Rev. B **49**, 3352 (1994).
47. I.A. Abrikosov, O. Eriksson, P. Söderlind, H.L. Skriver, and B. Johansson, Phys. Rev. B **51**, 1058 (1995).
48. R. Hayn and V. Drchal, Phys. Rev. B **58**, 4341 (1998).
49. I.A. Abrikosov, P. James, O. Eriksson, P. Söderlind, A.V. Ruban, H.L. Skriver, and B. Johansson, Phys. Rev. B **54**, 3380 (1996).
50. P. James, I.A. Abrikosov, O. Eriksson, and B. Johansson, in: Properties of Complex Inorganic Solids, edited by A. Gonis, A. Meike, and P.E.A. Turchi (Plenum Press, New York, 1997), p. 57.
51. J. Kudrnovský, I. Turek, A. Pasturel, R. Tetot, V. Drchal, and P. Weinberger, Phys. Rev. B **50**, 9603 (1994).
52. S.K. Bose, V. Drchal, J. Kudrnovský, O. Jepsen, and O.K. Andersen, Phys. Rev. B **55**, 8184 (1997).
53. J. Kudrnovský, I. Turek, V. Drchal, P. Weinberger, S.K. Bose, and A. Pasturel, Phys. Rev. B **47**, 16525 (1993).
54. I.A. Abrikosov and H.L. Skriver, Phys. Rev. B **47**, 16532 (1993).
55. J. Kudrnovský, V. Drchal, S.K. Bose, I. Turek, P. Weinberger, and A. Pasturel, Comput. Mater. Sci. **2**, 379 (1994).
56. I.A. Abrikosov, A.V. Ruban, H.L. Skriver, and B. Johansson, Phys. Rev. B **50**, 2039 (1994).
57. A. Christensen, A.V. Ruban, P. Stoltze, K.W. Jacobsen, H.L. Skriver, J.K. Nørskov, and F. Besenbacher, Phys. Rev. B **56**, 5822 (1997).
58. I. Turek, J. Kudrnovský, M. Šob, and V. Drchal, in: Stability of Materials, edited by A. Gonis, P.E.A. Turchi, and J. Kudrnovský (Plenum Press, New York, 1996), p. 431.
59. I. Turek, S. Blügel, and J. Kudrnovský, Phys. Rev. B **57**, R11065 (1998).
60. J. Kudrnovský, I. Turek, V. Drchal, P. Weinberger, N.E. Christensen, and S.K. Bose, Phys. Rev. B **46**, 4222 (1992).
61. M.V. Ganduglia-Pirovano, J. Kudrnovský, I. Turek, V. Drchal, and M.H. Cohen, Phys. Rev. B **48**, 1870 (1993).
62. J. Kudrnovský, I. Turek, V. Drchal, and P. Weinberger, Prog. Surf. Sci. **46**, 159 (1994).
63. I. Turek, J. Kudrnovský, M. Šob, V. Drchal, and P. Weinberger, Phys. Rev. Lett. **74**, 2551 (1995).
64. M.V. Ganduglia-Pirovano, J. Kudrnovský, and M. Scheffler, Phys. Rev. Lett. **78**, 1807 (1997).
65. J. Kudrnovský, S.K. Bose, and V. Drchal, Phys. Rev. Lett. **69**, 308 (1992).
66. A.M.N. Niklasson, I.A. Abrikosov, and B. Johansson, Phys. Rev. B **58**, 3613 (1998).
67. J. Kudrnovský, V. Drchal, I. Turek, P. Bruno, P. Dederichs, and P. Weinberger, these Proceedings.
68. O.K. Andersen, Z. Pawlowska, and O. Jepsen, Phys. Rev. B **34**, 5253 (1986).

69. Prabhakar P. Singh and A. Gonis, Phys. Rev. B **48**, 1989 (1993).
70. Prabhakar P. Singh and A. Gonis, Phys. Rev. B **48**, 2139 (1993).